Manuscript-ID: acp-2016-480

Dear Prof. Hoose,

following the comments from both reviewers, we improved our manuscript together with some additional changes.

The mayor changes are:

- In most parts we replaced 'convective mixing' by 'vertical mixing' to make it more clear that vertical mixing is the mayor point we want to investigate in our study. Our hypothesis H2, which assumes convection during the day, is only one possible explanation for vertical mixing but there might be other reasons for mixing as discussed in our manuscript.
- Changes of co-authors
- Update of POLIS profile in Sect. 4.1 (using less vertical smoothing and additional errorbars)
- Added lidar profiles from BERTHA in Sect. 4.1
- Added two further in-situ profiles in Sect. 4.2
- Removed average POLIS profile from Sect. 5
- Extended supplement
- Improved discussion and conclusions

Please find below the responses to the reviewers, followed by the manuscript with the highlighted changes since the published discussion paper (as produced by *latexdiff*). The revised manuscript and supplement are uploaded separately.

Thank you very much for handling the review process of our manuscript.

Kind regards,

Josef Gasteiger

Author's response to reviews of discussion paper 'Particle settling and convective mixing in the Saharan Air Layer as seen from an integrated model, lidar, and in-situ perspective' by Gasteiger et al. (acp-2016-480)

Reviewer comments are written in italic font, author's responses in normal font.

Response to reviewer 1

The paper tests two hypotheses about convective mixing within the SAL: one that assumes no mixing (H1), and the second that does assume mixing. This second hypothesis (H2) assumes heating due to absorption of sunlight by the dust particles, causing convective mixing during the day, and settling during the night. I think the paper is overall well written, especially the methods and model used are described in detail. However there are some issues that I want to discuss in the review below. The conclusion of this paper is that the scenario as modeled in H1 is unrealistic, leaving H2 to be the most viable option. A real-world scenario can't be as simple as described in H1. However, in many ways H2 also does not seem to be a perfect fit, and in the future perhaps more aspects of the model could be tested, to get insight in what determines the measured lidar profiles.

We thank reviewer 1 for his/her thoughtful comments that helped us to improve our manuscript.

Specific comments:

Comments described as page number/line number(s)

2/8: Why is particle size described here as radius? The cited reference (Maring et al., 2003) also uses particle diameter.

The reason is that radius is used more often than diameter in aerosol optical modeling and remote sensing, which is the research field our manuscript originates from. We think, as long as it is clearly stated which size description is used, this should be no issue for the reader.

3/2-3: Do you have a reference for this data collected during the SALTRACE field campaign?

We added here the reference to the SALTRACE overview paper (which is in review).

3/13: Six irregular dust particle shapes, is this enough to accurately represent Saharan dust?

This number of shapes certainly is not enough to accurately represent all aspects of Saharan dust. In real dust plumes, the number of shapes is 'almost infinite'. Nevertheless, the variability between these six dust-like shapes is large enough to cover the optical

properties of Saharan dust mixtures sufficiently well for the purpose of our study. We added a sentence claiming that using these six shapes is only an approximation.

The issue raised by the reviewer was the idea behind Figure 5. It shows that the linear depolarization ratio decreases towards the SAL top for each of the six very different dust-like shapes.

3/24: What is the particle density based on? Is there a reference for this?

The particle density assumption is based on Hess et al. (1998). We added this reference here.

3/24-25: What about the drag force of an aerosol particle larger than r = 10 μm? There are many studies that observe giant dust particles being transported from the Sahara over the Atlantic Ocean (e.g. (Glaccum and Prospero, 1980; Betzer et al., 1988; Goudie and Middleton, 2006; Mahowald et al., 2014; Middleton et al., 2001; Kok, 2011)).

For increasing size the Reynolds number, which is the ratio of inertial to viscous forces, increases (Hinds, 1999). The inertial forces become relevant for $r > 10$ μm, leading to a reduction of the settling velocity compared to Stokes which assumes only viscous forces. However this reduction becomes relevant only slowly: Using the formula given by Hinds, 1999, the Reynolds number for spheres with our assumed dust density of 2600 kg m^{-3} is $\approx$0.04 for r = 10 μm, $\approx$0.35 for r = 20 μm, $\approx$1.2 for r = 30 μm. According to the same book, the error of the drag force calculated by Stokes law is 5 % at Reynolds number 0.3 and 12 % at Reynolds number 1.0. Thus, if we extra-/interpolate between the Reynolds numbers and assume that the proportionality between drag force and velocity (Eq. 2 of discussion paper) is still valid in this size range, we can estimate that the settling velocity is reduced compared to Eq. 3 by about 5 % for r = 20 μm particles and about 15 % for r = 30 μm. In case of non-spherical particles things could be a bit more complicated, for example non-random orientation of giant dust particles may lead to a further reduction of the settling velocity (see response to reviewer 2). We now briefly discuss this in our article, but prefer not to go in too much detail because such giant dust particles are only of minor importance for our study.

5/Figure 2: Maybe this figure can be mirrored, so that it resembles the E-W transport over the Atlantic Ocean, as is described in the paper.

We prefer to keep the direction with increasing time towards the right because our model is based on time spans. To make it a bit easier for the reader to comprehend the relation to geography we added a few geographic names to the figure.

5/12: HSAL also decreases westward (Adams et al., 2012), which may affect the modeled results? (As also shown in in the supplementary data, Figure S-11).

The effect of considering a decrease of HSAL (e.g. HSAL = 4 km at the beginning and HSAL = 2 km in the Caribbean) would be that particle removal would be weaker at the beginning and stronger later. Replacing the fixed HSAL of 3 km by this westward decreasing HSAL (4 km before inight=2, 3.5 km before inight=3, etc.) changes δ_l at dz = 1 km from 0.29490 to 0.29459 for [H2, 6, 8h], and from 0.29854 to 0.29907 for [H2,

3, 8h]. However, in the paper we prefer to use only a single value for simplicity of our idealized model.

6/Figure 3: At inight = 0, the particle concentration of every size class is 1. Is this realistic, since particles are never distributed equally in any given sample? (e.g. (Stuut et al., 2005)). And are these number concentrations or volume/surface distributions?

The reviewer probably misinterpreted Fig. 3. Fig. 3 shows the fraction of particles existing in the SAL at the beginning of each night relative to the initial size distribution (reference ensemble described in the subsequent subsection). A fraction of 1 means that no particles had sedimented from the SAL. Thus, at i_{night}=1, the unmodified size distribution of the reference ensemble is used. In the subsequent night, for example, ≈50 % of the r = 12 μm particles are removed from the SAL (see green line in Fig. 3). This relative fraction could be applied to number, surface, volume distributions. In our case we apply it, following Hess et al. (1998), to dN/dr. We improved the description related to Fig. 3 to make it clearer.

6/6-7: Can you show the grain-size distributions that you have used in your model? What is the maximum grain size used?

We now added a figure in the supplement illustrating the number/surface/volume distribution of our reference ensemble, modified for different i_{night}. As maximum radius in the reference ensemble we use 40 μm, which is now mentioned in the paper. During the mixing-free time, the size distribution is cut off at the r_{max} given by Eq. 4.

7/15-16: Do you have a reference for this? E.g. Prospero (1996), Schütz (1980).

We now have added reference to Schütz (1980).

8/8-9: This may also be true for other aspects, like chemistry (and refractive index) and particle size. In how far have you tested how representative that data is for realistic cases?

The reviewer is correct in that this is certainly true also for refractive index and size distribution because of the quite complex nature of desert aerosol. We use refractive index data and size distribution data that is consistent with measurements near the source regions (and then modify the size distribution as function of transport time and height). So we think that it is 'sufficiently representative' for our study. We tested also the sensitivity of the depolarization ratio profile to realistic variations of refractive index and initial size distributions but we found that the sensitivity is lower than the sensitivity to particle shape (shown in Fig. 5). Now this is mentioned in the text.

9/14-17: Yes, there seems a minor effect when the shape conversion factor is taken as an average, but there is a substantial difference between the different shape mixtures (different colors in Fig. 6). What shape mixture was eventually used for the comparison with POLIS and CALIOP data?

We now better describe why we do this comparison. The purpose of showing different shape mixtures is to show that our results with respect to the relative importance of the settling-induced separation of particle size versus the separation of particle shape is not

specific to the reference ensemble. For the comparison with the measurements we use mixture BCDF (reference ensemble, shown as black lines), which was found to provide optical properties consistent with lidar measurements near the Sahara (Gasteiger et al., 2011).

10/10-11: Is there a reference that describes this field campaign and its data?

We added reference to the SALTRACE overview paper.

11/9-10: Why are the backward trajectories not shown? At what heights were the air layers modeled? Maybe satellite imagery can help to track the dust layer? (It seems like the dust was emitted at July 4th) see: https://worldview.earthdata.nasa.gov/

We now added backtrajectories to the supplement. As endpoint height we took the heights where the SAL was detected over Barbados (3.6, 4.0, 4.4 km in the plot added to the supplement). Emission on July 4th seems plausible to us. In H1 we assume that settling starts only when the SAL reaches the Atlantic, thus in Sect. 4 we need to look at this later point of time. If we would consider settling over Africa as well (meaning that we increase t_s in our model from 5 days to about 7 days) the depolarization curves for H1 would be shifted to larger dz (by a factor of 7/5). However, that would not change the conclusions of our paper.

11/18-19: Isn't the particle concentration measured as well? (Section 4.2, page 13) Can't that be used as input for the model?

Yes, the particle concentration was measured as well, however about 13 hours later. As the amount of particles strongly varies with time and location, these measurements can not be used as input here.

11/19-20: Why was the top of the SAL set at exactly 4660 m? What was this height based on? Based on the potential temperature it is said to be at 4600 m (11/13-14).

As we do have some spatial and temporal distance between the radiosonde and the lidar measurements, we assumed that the SAL top height could vary between lidar and radiosonde. The 4660 m was used because it best fits the H2 model to the measurements.

11/20: Why is a SAL height of 4740 m modeled? Apparently it matches the data better, but the data implies the top of the SAL may be at 4600 m (11/13-14), so maybe other parameters have to be adjusted to let the model better fit the data?

4740 m was selected to fit the H1 model to the measurements. Modifying shape, refractive index, size distribution does not help much to reduce the discrepancy between the SAL top height fitted to the POLIS data in case of H1 and the SAL top height measured by the radiosonde.

12/3-8: It seems that for the lower atmosphere, H1 fits better with the measurements, for both β and δ_l (Fig. 8b and 8c).

We agree. However, the upper part of the SAL is more sensitive to the discussed settling effects. In case of β we have to keep in mind that this is an extensive parameter, depending on the variable amount of particles. We now have reevalutated the POLIS

data using a reduced vertical smoothing range. The δ_l profile lies between H1 and H2 and the uncertainties of the measurements are in the same range as the differences between H1 and H2.

12/14-16: In the case of Fig 8, I don't see why H2 would fit better than H1.

Since we have no further information about the exact SAL top height during the lidar measurements, we now discuss this comparison saying that the lidar data does not fit better to one of our hypotheses.

13:5-6: This size range of 0.25-25 μm (radius), is this the same size range as used in the model?

No, this is a different size range. However, both size ranges cover the sizes of interest (see Fig. 1+2 and the new Fig. S-1 in the supplement).

13/8-9: '[. . .] allowing us to test more directly the size distributions resulting from our hypotheses H1 and H2.' Why not do this before the model calculations, and incorporate the data in the model?

In our current model it is not possible to incorporate the data collected over Barbados because our model needs the aerosol mixture at the start of the transport (i.e. data collected over Africa). Of course, we could show the in-situ data before the lidar data. But as both data sets are independent of each other, this would not change our conclusions.

13/10: Again, is there a reference for this aspect of the SALTRACE project that describes the data and how it was obtained? Because there are not many details about this in the current paper (e.g. location, flight plan, etc.)

More information is given in the SALTRACE overview paper. In addition, we added in the supplement a map where the locations of the measurements are illustrated.

13/11: '[. . .] the data was grouped in size ranges that are affected differently by particle settling.' What is this based on?

The nominal size bins are provided by the manufacturer of CAS-DPOL and the size ranges were selected based on Eq. 3 / Fig. 1 such that we expect a significant height dependence if H1 is true.

13/12-14: Why were these particle sizes considered? Why not the even coarser particles (up to $r = 25\ \mu m$)?

The counting statistics is gets low very quickly with increasing size and thus Poisson uncertainty gets very large (note the already large error-bars in Fig. 9 for the 'not-so-coarse' particles). As we investigate the height dependence, we have to use data from ascends and descends of the Falcon where the sampling time per height range is limited as described in the text.

14/1-3: Again, where is this effect of size on particle settling based on? What determines these boundaries?

We added reference to Eq. 3 and Fig. 1. These boundaries are selected from those provided by the manufacturer.

14/9: This seems like a very low amount of particles per size bin, how reproducible are these numbers? Have more of similar flights been performed in this area to compare the data to?

The limited reproducibility, as a result of the low number concentration of coarse particles, is related to the error bars shown in Fig. 9. These error bars show the range where the "real" ratio lies with 95 % probability.

We added two additional profiles from SALTRACE (22 June and 10 July). Our conclusions from the profiles with respect to H1 are the same as for 11 July.

14/22-23: If this data from SALTRACE is available, why not look at more case studies as in section 4? Since every case is unique, this could give more general insights in the processes involved during transportation of dust within the SAL, related to convective mixing. Why was the case of July 11th chosen for comparison with modeled data?

We had included a second case study in an earlier version of the manuscript. However we preferred to remove it because not much new insights could be gained from it. July 11th was chosen because of the favorable measurement conditions and a strong dust outbrake arriving over Barbados.

15/5-6: 'We again analyze the upper 1 km of the SAL [. . .]', I assume this was also done for averaging the POLIS data, however it is not mentioned in the previous section (5.1).

The reviewer's assumption is correct.

16/9-10: 'No significant differences in the average profiles were found between day- time and night-time data (not shown).' What does this tell us? That there seems to be convection during both night and day? (which is not assumed in your model)

Within the uncertainties of the measurements there seems to be no difference between day and night. This could mean that there is also vertical mixing during the night and settling during the day. However, given the uncertainties of the data we can not conclude on that.

17/19-23: To me it seems that the agreement between the POLIS data and H2 is also not good, just as the bad fit with H1. With the CALIOP data, however, the fit with H2 is much better.

Also the in-situ data can be much better explained with H2. The reason why we think H2 fits better with the averaged POLIS data was that the height dependence in the upper part (upper 100-200 m) of the SAL better agrees with H2 than with H1. We removed the average POLIS profile from the manuscript because the selection of the cases with a distinct SAL and the selection of its top height was done manually (and developing an objective approach for this procedure is a tricky task).

17/23-24: You seem to discuss the comparison between CALIOP and H2 also in the next paragraph, so maybe this sentence is a bit redundant here.

As this is a result we like to keep it here and to refer to the discussion in the next paragraph.

18/10-14: Could you say a bit more about the supplementary data? If not here, then in the supplement itself?

We extended the description in the supplement.

18/24-25: As mentioned for the previous sections as well, I think the results when comparing the model to POLIS data are not that conclusive, for both the case study and the average POLIS data.

The in-situ data looks more conclusive and the in-situ data was accounted for in this sentence. We are more specific now.

18/28-29: This relation with particle size isn't really mentioned in the discussion before (except for Figure 9).

We removed this sentence.

Technical corrections:

9/8: do you mean '[. . .] the importance of the shape dependence ON the gravitational settling for δ_l profiles.'?

We reformulated the sentence.

11/15: 'The relative humidity AT 4500 - 4600 m [. . .]'

Corrected.

16/Fig 10 (caption line 4): The statistical uncertainty of the mean, do you mean standard deviation? Also, in the text you refer to CALIOP data, however in the legend now it says CALIPSO, which is not very consistent.

It is the uncertainty of the mean value. The uncertainty of individual profiles is much larger, mainly because of low signal-to-noise ratios. We use the uncertainty provided by NASA for the individual profiles to estimate the uncertainty of the mean value. We now provide the formula used for the calculation of the uncertainty of the mean.

We corrected the legend.

Response to reviewer 2

The authors investigate processes affecting long-range particle transport in the Saharan Air Layer (SAL) by modeling aerosol property profiles for two scenarios: (1) gravitational settling only and (2) gravitational settling alternating with convective mixing in the SAL. Model results are compared with ground- and space-based lidar measurements as well as aircraft particle counter measurements to determine the most likely scenario.

The paper is overall very well written and a valuable contribution that is suitable for publication in ACP. Nevertheless, I have some comments (below).

We thank also reviewer 2 for his/her thoughtful comments that helped us to improve our manuscript.

(1) The authors initialize their model with a reference ensemble. As a result, there is no variation of the modeled profiles for different time periods (see for example Figures S-1 to S-5). Is there any way to initialize the model with measured profiles (for example using CALIPSO data) and then compute the profile changes based on the assumptions outlined in the model description?

In principle, the initial aerosol ensemble in our model could be modified as function of time (and source) if sufficient data about the aerosol near the source is available. In our case such data was not available thus we had to rely on data measured near the desert during SAMUM and before (as incorporated in OPAC) providing some 'typical desert aerosol'. As we need the microphysical properties of the initial aerosol ensemble, we can not use CALIOP data for this purpose. The CALIOP data doesn't provide enough information about the aerosols to invert their microphysical properties.

(2) The description of the computation of the fraction of removed particles (p. 5, l. 4-14) is not clear to me. I am not sure how Equation 5 has been derived and why H_scale has been set to 10 km. Some further detail might be beneficial. Also, it is said that f(r) is calculated for z_fallen(r) < H_SAL with H_SAL being the SAL depth. Have the authors considered a starting height of the particles (not all start from the top)? In the context of l. 4 on p. 5, it might also be worth stating that only one air parcel (vertically reaching throughout the SAL) is considered and horizontal mixing is being ignored.

In our model not all particles start from the top. At start the particles are distributed over the complete (well-mixed) layer. We improved the description and hope it is clearer now. Furthermore, we found an error in the description of Eq. 5 (it calculates the fraction remaining in the SAL, not the fraction removed)

(3) Two hypotheses are considered: (H1) profile changes are caused by gravitational settling only; and (H2) profile changes are caused by gravitational settling during the night and convective mixing during the day. Do I understand correctly, that gravitational settling is being neglected during the day in H2? I would think that gravitational settling occurs always, irrespective of whether or not convective mixing occurs in addition. Looking at Fig. 10, I could imagine that the additional consideration of daytime gravitational

settling in H2 might reduce delta_l at large heights (small dz) and thus lead to a smoother profile which compares better to the measured profiles.

Yes, gravitational settling is neglected during the day in H2. We agree that consideration of settling and imperfect mixing during the day should improve the agreement in Fig. 10. To consider this, we would have to add some parameterization of the strength of the vertical mixing as function of dz. However, we prefer not to further extend our model in the current work, for which the main conclusion is that assuming no vertical mixing of air (H1) is unrealistic. But in future work it seems natural that our, still very idealized, H2 could be replaced by a more realistic model for the SAL.

(4) The cross-sectional particle radius, r_c, is being used for the computation of the drag force (Section 2.1). However, r_c varies with particle orientation. Has this been accounted for in the model? As the authors assume a random particle orientation, the drag force might have to be calculated as an average over the drag force of single particles with different orientation. Is there any information about whether or not particles are being oriented randomly in nature or if the perhaps align with the flow in some way?

The reviewer is right in that calculating the drag force for average r_c could differ from the average over the drag force of a single particle in different (random) orientation. However, because of F_d being proportional to r_c (Eq. 2) the difference between both approaches should be rather small.

Small particles usually have random orientation due to Brownian motion. If non-spherical particles are larger, they have the tendency to orient horizontally while sedimenting (i.e. with their larger cross section against the flow). Now after the reviewer's comment we searched the available literature to estimate at which size the particle orientation might become non-random. We found the paper of Ulanowski et al. (2007, doi: 10.5194/acp-7-6161-2007) to provide the required formula. In Fig. 9 of their paper they show that (in the absence of an electric field, 0 V/m) the orientation becomes non-random for prolate spheroids with aspect ratio 1.5 if the maximum particle dimension reaches 10 micrometers. Using their Eq. 14 and 16 and our Eq. 3 we calculated the mean angle for prolate spheroids with different aspect ratios, as function of r_c and plot it in the following figure:

It shows that the mean angle does not depend very much on the aspect ratio. Assuming that real dust particles (with average aspect ratio 1.6-1.8) behave similar to prolate spheroids we estimate that the transition region between random and non-random orientation is at about $r_c = 5$ μm.

Preferred horizontal orientation would lead in tendency to a reduction of the settling velocity because of increased drag compared to the drag for random orientation. In the book 'Bubbles, drops, and particles' by Clift et al. formulas are provided allowing us to calculate the ratio between the drag force of spheroids in horizontal orientation and the drag force in random orientation. In case of oblate spheroids this ratio is about 1.09 and 1.15 for aspect ratios 1/2 and 1/3, respectively. For prolate spheroids we find ratios of 1.06 and 1.12 for aspect ratios 2 and 3, respectively. Unfortunately, we have

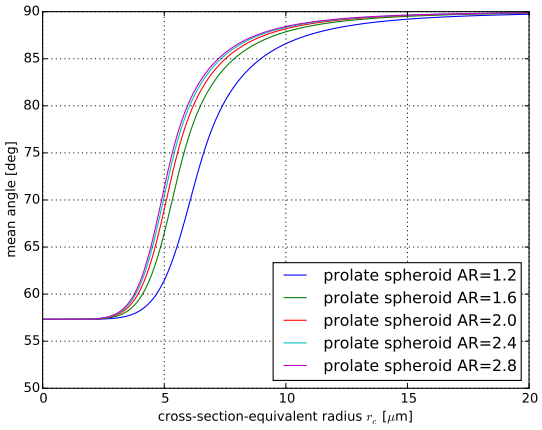

no further information for the case of irregular particle shapes. Given the available information (including the information that average dust aspect ratios are around 1.6-1.8) we estimate that in reality the average settling velocity of desert dust particles at r $>$ 5 μm might be, on average, 5 % smaller in case of horizontal orientation (compared to random orientation). As this reduction does hardly change the modeled lidar profiles we only briefly mention this effect in the paper but do not consider it in the calculations.

(5) The authors suggest that convective mixing in the SAL occurs due to 'absorption of sunlight by the aerosol particles'. Would this not lead to stronger heating at the top of the SAL compared to the bottom and thus to a stabilization?

Yes, as the sunlight becomes weaker towards the bottom of the layer a stabilization should be expected. On the other side, if particle settling had started, the amount of absorbers gets lower near the top, which reduces the heating there. Thus, sunlight could lead to a destabilization of the upper part of the SAL under certain conditions.

The main purpose of H2 is to contrast the scenario with no vertical mixing (H1) showing that some kind of vertical mixing occurs in the SAL. H2 probably is not fully realistic and mechanisms other than absorption of sunlight could be relevant for the vertical mixing in nature, as discussed towards the end of the paper. We modified the manuscript (including the title) to make the purpose of the paper more clear.

(6) Oceanic measurements (e.g. van der Does et al. 2016 [http://www.atmos-chem-phys-discuss.net/acp-2016-344/]) suggest, that particles of a few tens of microns can still be transported some distance across the Atlantic. Do the authors have any evidence of this from their measurements? If that is the case, then the Stokes regime might not apply anymore (for the largest particles). How would this affect the modeled profiles?

As the number concentration of such large particles is very low, lidar measurements are not sensitive to them and airborne in-situ measurements need a long sampling time to get good statistics about their abundance. However, the airborne in-situ measurements collected during SALTRACE near Barbados suggest that a few particles with diameters

around 30 micrometers arrive in the SAL at that location. For the possibility of transport of 'giant particle' over such long distances we like to refer to our response to reviewer 1 with respect to the error of the Stokes law, to the orientation effects discussed above, to Fig. 3 of our paper, and to the fact that 'extreme shapes' (with small ξ_{vc}) could 'survive' longer than those considered in our paper. As the sensitivity of lidar to 'giant particles' is low, the discussed uncertainties about these 'giant particles' hardly affects the modeled profiles.

Minor comments:

(1) P. 2, l. 9-10; To me, the statement 'cannot explain their measurements with Stokes gravitational settling alone' suggests that Stokes settling might be too weak. However, the subsequent statement, that they had to 'reduce the Stokes settling velocity' suggests otherwise. Perhaps rephrasing would clarify this.

We clarified this sentence.

(2) P. 3, l. 27; Suggest using half-blanks between unit-parts to avoid Pa (times) s being read as Pas.

Improved.

(3) P. 4, l.1; Setting F_g = F_d suggests that a particle would be suspended and not that it would be in 'still air', would it? Unless still air is interpreted such that the particle experiences no vertical movement.

We made this sentence more clear by writing "... results in a settling velocity of the particle relative to the ambient air of ...".

(4) P. 6, l. 10; Suggest using micrometers instead of nanometers for consistency.

Changed.

(5) P. 7, l. 27; The sentence 'We find a decrease of linear depolarization ratio delta_l with height' is somewhat confusing as it is not clear if the authors mean with decreasing or increasing height (or dz). Perhaps reword. This occurs also at other places in the paper (e.g. p. 9, l.4)

We changed throughout the paper as suggested by the reviewer.

(6) P. 9, l. 2; Please clarify which 'smaller-scale features' are meant.

With 'smaller-scale feature' we refer to the local maximum of δ_l for shape A at dz=100m. However, as this is not an important aspect of the manuscript, we removed this sentence.

(7) P. 9, l.9; Why do two particle shapes need to be mixed within one ensemble? Could the shape-dependence of settling not be investigated using two model ensembles each having only particles of a particular shape? (Perhaps I misunderstood the sentence).

No, this is not possible as we want to investigate the importance of the shape-dependence of settling velocity, which could lead to a shape separation of an initially well-mixed aerosol as suggested by Yang et al. (2013, doi: 10.1002/grl.50603). We try to explain this better now.

(8) P. 12, l.1; Suggest moving '(thin red line)' to after 4740 m.

Changed.

(9) P. 17, l.25; is instead of in

Corrected.

Particle settling and ~~convective~~ vertical mixing in the Saharan Air Layer as seen from an integrated model, lidar, and in-situ perspective

Josef Gasteiger[1,2], Silke Groß[3], Daniel Sauer[3], Moritz Haarig[4], Albert Ansmann[4], and Bernadett Weinzierl[2]

[1]Meteorologisches Institut, Ludwig-Maximilians-Universität, München, Germany
[2]Faculty of Physics, University of Vienna, Vienna, Austria
[3]Institut für Physik der Atmosphäre, Deutsches Zentrum für Luft- und Raumfahrt, Oberpfaffenhofen, Germany
[4]Leibniz Institute for Tropospheric Research, Leipzig, Germany

Correspondence to: Josef Gasteiger (josef.gasteiger@univie.ac.at)

Abstract.

Long-range transport of aerosol in the Saharan Air Layer (SAL) across the Atlantic plays an important role for weather, climate, and ocean fertilization. However, processes occurring within the SAL and their effects on aerosol properties are still unclear. In this work we study particle settling and ~~convective~~ vertical mixing within the SAL based on measured and modeled vertical aerosol profiles in the upper 1 km of the transported SAL. We use ground-based ~~POLIS~~ lidar measurements and airborne particle counter measurements over the Western Atlantic, collected during the SALTRACE campaign, as well as space-based CALIOP lidar measurements from Africa to the Western Atlantic in the summer season. In our model we take account of the optical properties and the Stokes gravitational settling of irregularly-shaped Saharan dust particles.

We test two hypotheses about the occurrence of ~~convective~~ vertical mixing within the SAL over the Atlantic to explain the aerosol ~~properties~~ profiles observed by the lidars and the particle counter. Our first hypothesis (H1) assumes that no mixing occurs in the SAL leading to ~~an altitude separation of super-micron dust particles as a result of settling~~a settling-induced separation of particle sizes. The second hypothesis (H2) assumes that ~~convective~~ vertical mixing occurs in the SAL ~~during the day~~ allowing large super-micron dust particles to stay airborne longer than without ~~convective~~ mixing.

~~In general, a decrease~~ The uncertainties of the particle linear depolarization ratio ~~towards the SAL top is found in the measured lidar data but the decrease is much weaker than modeled in case of~~ (δ_l) profiles measured by the ground-based lidars are comparable to the modeled differences between H1 ~~. The~~ and H2 and do not allow us to conclude which hypothesis fits better. The SALTRACE in-situ data on particle number concentrations show a presence of large particles near the SAL top that is inconsistent with H1. ~~Furthermore,~~ Also the analysis of the CALIOP measurements reveals that the average ~~vertical profile of the linear depolarization ratio of the aerosols~~ δ_l profile over the Western Atlantic is inconsistent with H1. Furthermore, it was found that the average δ_l profile in the upper 1 km of the SAL does not change along its transport path over the Atlantic. These findings ~~indicate H2 to be much more likely than H1, giving evidence that convective mixing occurs~~ give evidence that vertical mixing within the SAL ~~over the Atlantic~~ is a common phenomenon with significant consequences for the evolution of

the size distribution of the super-micron dust particles during transport over the Atlantic. Further research is needed to precisely characterize the processes that are relevant for this phenomenon.

1 Introduction

The Saharan Air Layer (SAL) carries large amounts of Saharan aerosol particles towards the Western Atlantic Ocean and the Americas, in particular during summer time (Prospero and Carlson, 1972; Carlson and Prospero, 1972; Schütz, 1980) (e.g., Prospero and C The SAL over the African continent often is a well-mixed convective layer from the hot surface to about 4-6 km above sea level (Ben-Ami et al., 2009; Knippertz et al., 2009; Cuesta et al., 2009; Esselborn et al., 2009). As soon as the SAL reaches the Atlantic, it is lifted over a comparatively cold marine boundary layer. As a consequence, the radiative heating at the bottom of the SAL, which is a strong driving force for convection, vanishes. However, weaker convection vertical mixing within the SAL over the Atlantic might be possible due to other radiative or dynamic effects. Knowledge about those processes is quite limited but they can be important for the evolution of the particle size distribution during transport. Changes in size distribution can have significant effects for radiative properties and deposition of Saharan aerosols (e.g., Otto et al., 2009; Mahowald et al., 2014).

Size distribution measurements performed at Izaña (Canary Islands) and Puerto Rico (Caribbean) by Maring et al. (2003) revealed that Saharan dust particles with $r > 3.6$ µm are preferentially removed during the transport over the Atlantic. Maring et al. (2003) cannot explain their measurements with by assuming that Stokes gravitational settling alone, but they is the only process occurring during transport over the Atlantic. They have to reduce the Stokes settling velocity by 0.0033 m s^{-1} to match the measurements. This , which could be an indication for vertical mixing of air during the transport. Also the lack of significant vertical changes of particle size distributions found by Reid et al. (2003) in the Caribbean indicate that settling is counteracted by some other processes.

Lidar remote sensing is a powerful tool to localize and characterize aerosols, including their size distributions. The particle linear depolarization ratio δ_l (Sassen, 1991), measured by advanced lidar systems, is a particularly useful parameter to characterize Saharan aerosols. For example, Liu et al. (2008) characterize in a case study a dust outbreak that was transported from the Sahara over the Atlantic. They use measurements of the CALIOP lidar (Winker et al., 2009), which is operated on-board the CALIPSO satellite and measures δ_l at a wavelength of 532 nm. Liu et al. (2013) investigate Asian dust and its transport over the Pacific using data from the same instrument. The network EARLINET (Pappalardo et al., 2014) provides a comprehensive data set on ground-based lidar measurements throughout Europe, which is useful to study Saharan aerosols transported to Europe (see e.g., Mattis et al., 2002; Papayannis et al., 2008; Wiegner et al., 2011). During field campaigns like PRIDE (Reid et al., 2003), SAMUM (Heintzenberg, 2009; Ansmann et al., 2011), Fennec (Ryder et al., 2013) , and SALTRACE (Weinzierl et al., 2016), Saharan aerosol has been measured using a wide set of techniques, including lidar, photometer, and airborne in-situ instrumentation. The combination of different measurement techniques enables one to better constrain the properties of the rather complex Saharan aerosol. Polarization-sensitive (near-)backscattering by dusty aerosols is studied also in laboratories (e.g., Sakai et al., 2010; Järvinen et al., 2016).

Yang et al. (2013) investigate Saharan aerosols on their way over the Atlantic based on δ_l data from CALIOP. They use δ_l from volumes that the CALIPSO operational algorithm classified as dust-laden and average δ_l, as function of height above sea level, over the summer season 2007. The averaged δ_l profiles show an increasing height dependence with increasing distance from Africa. In the Western Atlantic they find the largest δ_l values at altitudes of about 4-5 km and a decrease of δ_l with decreasing altitude. Yang et al. (2013) explain the averaged CALIOP δ_l profiles with ~~shape-induced gravitational sorting using a simple~~ settling-induced separation of particle shapes using a model which assumes that particles with nearly spherical shape ~~fall~~ settle faster and have smaller δ_l than particles with stronger deviation from spherical shape.

In our study we investigate the Saharan aerosol transport over the Atlantic by combining advanced modeling efforts with data obtained from ground-based lidar, from airborne particle counters, and from the CALIOP lidar. We show theoretical profiles for Saharan aerosols considering gravitational settling as function of particle size and shape, and two hypotheses about the occurrence of ~~convective~~ vertical mixing within the SAL. The lidar-relevant optical properties are simulated based on the particle microphysics explicitly using an optical model. We compare our modeled profiles with the measured data that we evaluate as function of distance from the SAL top. The ground-based and airborne measurements used in our study were performed during the SALTRACE field campaign ~~in~~ (Weinzierl et al., 2016) in the summer 2013 in the vicinity of Barbados (Caribbean). From CALIOP, we use night-time profile data covering 15 summer months and the Saharan aerosol transport region from Africa to the Caribbean.

After describing our modeling approach (Sect. 2) we investigate modeled lidar profiles after five days of transport without ~~convective~~ vertical mixing (Sect. 3.1), which is a typical transport time of Saharan aerosol to the Caribbean. The sensitivity of δ_l profiles to particle shape (Sect. 3.2) and to the shape dependence of the settling velocity (Sect. 3.3) is investigated subsequently. In Sect. 3.4 we model the effect of day-time convective vertical mixing occurring in the SAL during transport. Subsequently, the modeled profiles are compared in a case study to lidar and in-situ profiles measured in Barbados during SALTRACE (Sect. 4) to test our two hypotheses about ~~convection~~ vertical mixing in the SAL over the Atlantic. In Sect. 5 we continue testing these hypotheses by using averaged ~~SALTRACE lidar profiles and averaged CALIOP profiles.~~ CALIOP profiles, before we give concluding remarks in Sect. 6.

2 Model description

Our model describes Saharan aerosols in the SAL. We consider six irregular dust particle shapes, as introduced by Gasteiger et al. (2011), with shapes A-C being deformed prolate spheroids with varying aspect ratio, shape D an aggregate, and shapes E-F edged particles with varying aspect ratio (these shapes are depicted further down in Fig. 5 ~~).~~ together with their aspect ratios). Though this low number of model shapes is not sufficient to represent all aspects of Saharan dust in full detail, model ensembles composed of these dust shapes and small water-soluble particles can be used to approximate optical properties of Saharan aerosols (Gasteiger et al., 2011) . We assume the particles to be randomly oriented. We furthermore assume that the SAL initially is well-mixed and that gravitational settling of the aerosol particles is the only process when ~~convective mixing is stopped~~no vertical mixing occurs. We also consider the case of a diurnal cycle of the convective mixing activity.

2.1 Stokes settling

The settling velocity v of a particle relative to the ~~surrounding~~ ambient air is determined ~~mainly~~ by the balance between gravitation force F_g and drag force F_d if other forces can be neglected. The gravitation force is given by

$$F_g = \frac{4}{3}\pi {r_v}^3 \rho g \tag{1}$$

with the volume-equivalent radius r_v of the particle, the gravitational acceleration $g = 9.81$ m s^{-2}, and the particle density ρ that we assume to be $2.6 \cdot 10^3$ kg m^{-3} for ~~desert dust particles~~ mineral dust particles (Hess et al., 1998) . The drag force of ~~an~~ a settling aerosol particle in the size range from $r \approx 0.5$ µm to $r \approx 10$ µm (being in the Stokes' drag regime) can be approximated by

$$F_d = 6\pi\eta r_c v \tag{2}$$

with the dynamic viscosity of air $\eta = 17$ µPa s (approx. value for a temperature of 0°C ~~temperature~~ and tropospheric pressures) and the cross-section-equivalent radius r_c of the particle. We use r_c instead of r_v in this equation because the drag force is related more to the cross section of the particle than to its volume. ~~However, we~~

We note that using r_c in Eq. 2 is an approximation because determining the exact Stokes drag force of an irregularly-shaped particle is a more complex issue, see e.g. Loth (2008). ~~Setting F_g =~~The drag force of a particle larger than $r \approx 10$ µm is stronger than calculated with Eq. 2. For example in case of spherical particles, F_d is increased by about 5 % for $r = 20$ µm and about 15 % for $r = 30$ µm compared to Stokes law (Hinds, 1999) . In addition, because of the flow around the settling particle, coarse non-spherical particles can become horizontally aligned. Using the formula about the probability distributions of orientation angles of prolate spheroids compiled by Ulanowski et al. (2007) , we estimate that settling-induced alignment occurs for dust particles with $r > 5$ µm. In the Stokes regime, for typical dust aspect ratios of 1.6-1.8, F_d of a spheroid in horizontal orientation is on average about 5 % stronger than the average F_d of the same particle in random orientation (Clift et al., 1978) . In the following, we stick to Eq. 2 for the calculation of F_d because these deviations have only negligible effect on the profiles presented below.

Setting $F_g = F_d$ and using the conversion factor $\xi_{\mathrm{vc}} = r_v / r_c$ (Gasteiger et al., 2011) results in a settling velocity of the particle ~~in still~~ relative to the ambient air of

$$v = \frac{2g\rho}{9\eta} \cdot r_c^2 \cdot \xi_{\mathrm{vc}}^3 \tag{3}$$

ξ_{vc} of our six irregular model shapes are 0.955 (shape A), 0.932 (B), 0.911 (C), 0.871 (D), 0.925 (E), and 0.866 (F). Note that the dynamic shape factor χ (Hinds, 1999) is $\chi = \xi_{\mathrm{vc}}^{-1}$ if r_v is assumed, and $\chi = \xi_{\mathrm{vc}}^{-3}$ if r_c is assumed for the radius. Henceforth unless otherwise stated, we use the cross-section-equivalent radius $r = r_c$ for describing particle size.

As a result of gravitational settling during a time period t_s without ~~convective~~ vertical mixing, the maximum particle radius r_{max} at a distance dz from the upper boundary of the SAL is given by

$$r_{\mathrm{max}} = \sqrt{\frac{9\eta dz}{2g\rho\xi_{\mathrm{vc}}^3 t_s}} \tag{4}$$

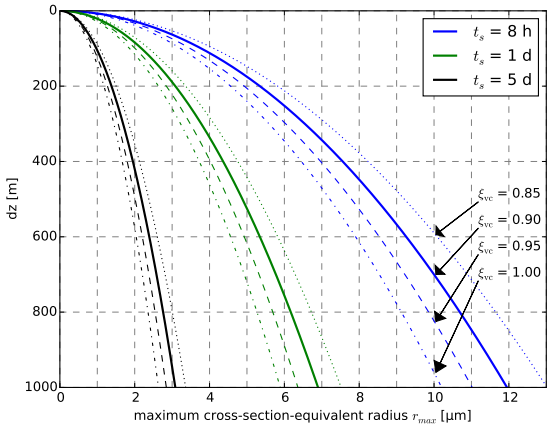

Figure 1. Maximum cross-section-equivalent radius $r_{\max}$ of dust particles as function of distance dz from the SAL top after different settling time periods t_s assuming different shape-dependent conversion factors ξ_{vc}. ξ_{vc} = 1 corresponds to spherical particles.

Fig. 1 illustrates $r_{\max}$ as function of dz for different settling time periods t_s. The solid lines show $r_{\max}$ for a conversion factor $\xi_{\mathrm{vc}} = 0.9$, which is in the range of our dust model shapes. The vertical axis was chosen such that the top of the SAL (dz = 0 m) is at the top of the figure. For example, at t_s = 5 d, no particles with radii $r > 2$ µm and $\xi_{\mathrm{vc}} = 0.9$ exist in the upper 400 m of the SAL.

2.2 Hypotheses about occurrence of ~~convective~~ vertical mixing

~~Schematic view of hypotheses about the occurrence of convective mixing within the SAL.~~

In our first hypothesis (H1) we assume that no ~~convective mixing~~ vertical mixing of air occurs in the SAL over the Atlantic. By contrast, in our second hypothesis (H2) we assume a diurnal cycle of the convection activity. The idea behind H2 is that the SAL is heated by absorption of sunlight by the aerosol particles triggering convective mixing during the day. In nature the physics behind vertical mixing of SAL air might differ from what we assume in our idealized model H2 (see discussion). The possibility of ~~convective~~ vertical mixing in the SAL is consistent with the ~~mostly~~ almost height-independent potential temperature profiles observed within the SAL (see e.g. Carlson and Prospero (1972) or further down on Fig. 8). We emphasize that the convection activity studied here is not connected to the convection occurring in the marine boundary layer (which sometimes affects ~~also the lower-most~~ the lower parts of the SAL).

Both hypotheses are illustrated in Fig. 2. We model the transport for one vertical column, ignoring possible wind shear or convergence. For simplicity, we assume that the SAL reaches the Atlantic at first sunset. Furthermore, we assume convective mixing always to be perfect though in reality convection may be weak and the vertical mixing imperfect. In case of H2, the initial aerosol size distribution at t_s = 0 varies from night to night because a certain fraction of particles is removed by settling during the convection-free time each night before convective mixing starts again with sunrise. The fraction f of particles ~~with~~

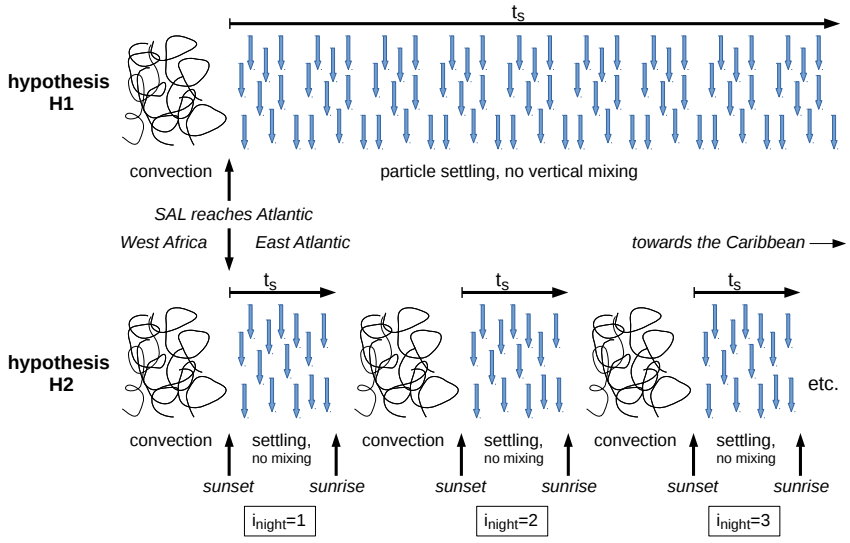

Figure 2. Schematic view of timing in hypotheses about the occurrence of settling and convective vertical mixing within the SAL.

~~radius r that is removed from the SAL each~~ that remains in the SAL after one night is calculated for ~~$z_{\mathrm{fallen}}(r)$~~ $z_{\mathrm{settled}}(r,\xi_{\mathrm{vc}}) < H_{\mathrm{SAL}}$ ~~with~~ using

$$f(r,\xi_{\mathrm{vc}}) = \frac{exp\left(\frac{H_{\mathrm{SAL}}-z_{\mathrm{fallen}}(r)}{H_{\mathrm{scale}}}\right)-1}{exp\left(\frac{H_{\mathrm{SAL}}}{H_{\mathrm{scale}}}\right)-1} \frac{exp\left(\frac{H_{\mathrm{SAL}}-z_{\mathrm{settled}}(r,\xi_{\mathrm{vc}})}{H_{\mathrm{scale}}}\right)-1}{exp\left(\frac{H_{\mathrm{SAL}}}{H_{\mathrm{scale}}}\right)-1} \tag{5}$$

where ~~$z_{\mathrm{fallen}}(r)$~~ $z_{\mathrm{settled}}(r,\xi_{\mathrm{vc}})$ is the distance the particles have ~~fallen (with~~ settled during the night. No particles with $z_{\mathrm{settled}}(r,\xi_{\mathrm{vc}}) > H_{\mathrm{SAL}}$ are in the SAL after the first night. z_{settled} is calculated using v ~~as given by~~ from Eq. 3 ~~) during the night . The duration of the night is set to~~ and a night duration of 11 h~~in our model~~, which is a typical value for the northern tropical Atlantic during summertime. H_{SAL} is the depth of the SAL within which convective mixing occurs each day. We use H_{SAL} = 3 km. ~~To consider the height dependence of the particle concentration present in case of~~ In Eq. 5 we assume that the particles are well-mixed ~~layers (as a result of the decrease of air density with height), we~~ within the SAL at sunset. Those particles that settle during the night below the lower boundary of the SAL (determined by H_{SAL}) are considered as removed from the SAL at sunrise when mixing starts again. Eq. 5 considers the exponential decrease of the air density, and thus the amount of aerosol (in case of well-mixed layers) with height. We assume a scale height H_{scale} = 10 km, which implies an exponential decrease by a factor of e from the ground to 10 km height. This value of H_{scale} was estimated from the tropical standard atmosphere provided by Anderson et al. (1986) .

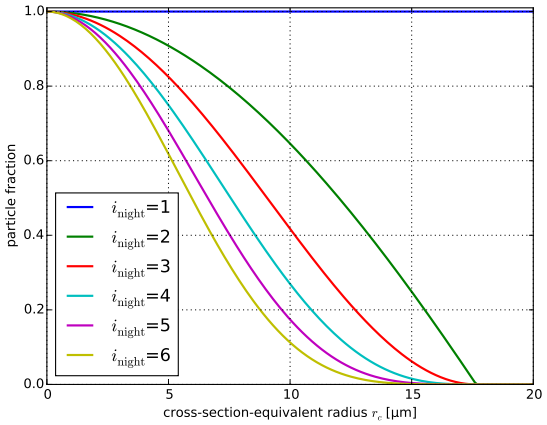

Figure 3. Fraction of particles (relative to initial size distribution) existing in SAL at beginning of each night ($t_s = 0$) in case of H2 and $\xi_{\mathrm{vc}} = 0.90$.

Figure 3 shows for H2 the fraction of the particles present in the SAL at the beginning of each night (counted by i_{night} as illustrated in Fig. 2). This fraction is calculated ~~as~~ from Eq. 5 using

$$(1 - f f(r), \xi_{\mathrm{vc}})^{(i_{\mathrm{night}}-1)} \tag{6}$$

and is multiplied with the initial aerosol size distribution, which is described below, to get the size distribution at the beginning of each night.

Henceforward in this paper, we denote the hypotheses and points of time using the following notation: For the first hypothesis we write [H1, t_s] and for the second hypothesis we write [H2, i_{night}, t_s].

2.3 Aerosol mixtures and optical modeling

We simulate the optical properties of Saharan aerosols based on their microphysical properties (size, shape, refractive index) as described by Gasteiger et al. (2011) and use the reference ensemble described in that contribution as the initial aerosol ensemble at [H1, 0 h] and [H2, 1, 0 h]. The lidar-related optical properties of this ensemble are consistent with measurements of Saharan aerosols over Africa (Gasteiger et al., 2011). The aerosol ensembles consist of four log-normal size modes ~~according to the 'desert mixture' of OPAC (Hess et al., 1998)~~ with one mode of small ~~spherical~~ water-soluble (WASO) particles ~~at 50% r.h.~~($\rho = 1.42 \cdot 10^3$ kg m^{-3}) and three modes of ~~non-spherical~~ mineral dust particles, as defined for the desert mixture in OPAC (Koepke et al., 2015) . For WASO particles, spherical shape, a relative humidity of 50 %, and a density of $\rho = 1.42 \cdot 10^3$ kg m^{-3} is assumed. Mixing of mineral dust with WASO particles is consistent with results presented by Kaaden et al. (2009) who ~~identified~~ found that Saharan aerosol particles in the smaller size ranges ($r <$ ~~100-250 nm) to~~ 0.1-0.25 µm) consist mainly of ammonium sulfate. Volatile ammonium sulfate particles were ~~also identified~~ identified also in airborne in-situ measurements ~~(Weinzierl et al., 2009)~~ during SAMUM (Weinzierl et al., 2009) and SALTRACE (Weinzierl et al., 2016) .

The mineral dust particles of the reference ensemble are an equiprobable mix of shapes B, C, D, and F (Gasteiger et al., 2011). The optical properties of dust particles with $2\pi r_v/\lambda \leq 25$ were calculated with the discrete dipole approximation code ADDA (Yurkin and Hoekstra, 2011) and for larger particles it was assumed that the lidar ratio S and the linear depolarization ratio δ_l are size-independent, i.e. S and δ_l calculated for $2\pi r_v/\lambda = 25$ was applied also for larger particles.

It has been shown for Saharan aerosols that the refractive index varies from ~~particle to~~ dust particle to dust particle (e.g., Kandler et al., 2011), and that this variability can have significant effects on lidar-relevant optical properties (Gasteiger et al., 2011). In our model, we consider the refractive index variability by the following approximating approach: The imaginary part of the dust refractive index, which is relevant for absorption, is distributed such that 50 % of the dust particles are non-absorbing while the other 50 % have an imaginary part that is doubled compared to the value provided by OPAC, leading to good agreement with SAMUM lidar measurements (Gasteiger et al., 2011).

We apply a maximum cut-off radius $r_{\max}$ that is varied as function of distance dz from the SAL top as given by Eq. 4. The maximum $r_{\max}$ is 40 µm (at $dz \leq 1$ km only relevant for $t_s < 1$ h). In case of a diurnal cycle of convective mixing (H2), we consider in addition the partial removal of particles due to settling each night, as described above (Eq. 6, Fig. 3). The evolution of the mineral dust size distribution for H2 (each night at t_s = 0) is illustrated in the supplement S-1.

We simulate vertical profiles of the extinction coefficient α, the backscatter coefficient β, the lidar ratio

$$S = \frac{\alpha}{\beta} = \frac{4\pi}{\omega_0 F_{11}(180°)} \tag{7}$$

and the linear depolarization ratio

$$\delta_l = \frac{1 - F_{22}(180°)/F_{11}(180°)}{1 + F_{22}(180°)/F_{11}(180°)} \tag{8}$$

Here, ω_0 is the single scattering albedo of the aerosol particles, $F_{11}(180°)$ and $F_{22}(180°)$ are elements of their scattering matrix at ~~backscattering~~ backward direction. We consider the height dependence of the particle concentration of the initially well-mixed layer by multiplying all modeled α and β profiles with $\exp(dz/H_{\text{scale}})$. In this paper, α, β, S, and δ_l are always aerosol particle properties, i.e. without gas contributions.

3 Modeled lidar profiles

In this section we first present modeling results for our first hypothesis (H1) with a settling duration of t_s = 5 d, which is the typical time span for transport of aerosol in the SAL from ~~Africa to the Western Atlantic~~the African coast to Barbados (e.g., Schütz, 1980) . H1 is selected here because the effects are stronger than in case of H2. We investigate the sensitivity of the δ_l profile ~~shape~~ to the particle shape and the ~~shape-dependent settling velocity~~ shape dependence of the settling velocity v. Finally in the last part of this section, we investigate the effect of ~~a diurnal convection~~ the diurnal convective mixing cycle (H2) on the δ_l profile.

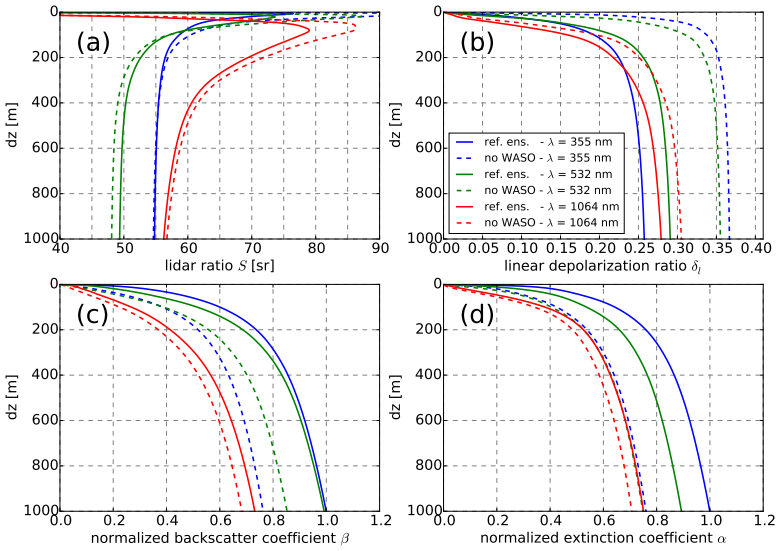

Figure 4. Optical aerosol properties of the upper 1 km of the SAL for [H1, 5 d] assuming the reference ensemble (solid lines) at three lidar wavelengths (indicated by color). β and α are normalized to the value of the reference ensemble at λ = 355 nm and dz = 1000 m. The dashed lines present profiles when WASO particles are removed from the reference ensemble.

3.1 Effect of particle settling (H1)

Vertical profiles of lidar-relevant optical properties of the aerosol in the upper 1 km of the SAL, modeled according to H1 after five days without ~~convective mixing (t_s =~~ vertical mixing of air ([H1, 5 d]), are shown in Fig. 4. The solid lines show results for the reference ensemble at three different lidar wavelengths (indicated by color). To illustrate the effect of the WASO particles, we also consider a case in which we removed all WASO particles (dashed lines of same colors).

The lidar ratio S increases towards the top of the SAL (Fig. 4a). S at λ = 532 nm and 1064 nm has peaks of about 75-80 sr in the upper 70 m of the SAL, decreasing again on the last few meters below the SAL top. Removing the WASO particles from the ~~reference~~ ensemble has a significant effect on S only near the top of the SAL (compare dashed with solid line).

We find a decrease of the linear depolarization ratio δ_l with ~~height~~ decreasing distance dz from the SAL top (Fig. 4b). The absolute decrease of δ_l depends on wavelength; for example, from dz = 1000 m to dz = 100 m δ_l decreases by 0.065, 0.074, and 0.121 at λ = 355 nm, 532 nm, and 1064 nm, respectively. Removing WASO particles strongly increases δ_l at all heights, in particular at short wavelengths (compare blue lines for λ = 355 nm)~~. However, the general shape of the~~ , illustrating their importance in modeling δ_l ~~profiles, i.e. the~~ of Saharan aerosols. The decrease of δ_l ~~with height, is independent of whether WASO particles are considered or not~~ is shifted towards smaller dz if WASO is neglected but the general shape of the δ_l profiles does not change.

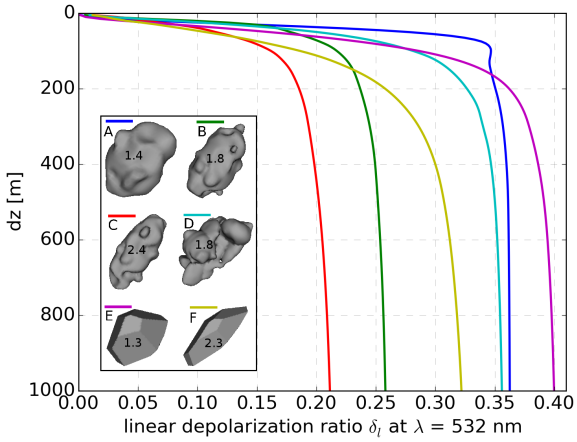

Figure 5. Linear depolarization ratio profiles at λ = 532 nm in the upper 1 km of the SAL for [H1, 5 d]. The reference ensemble is applied (as in Fig. 4), but only a single dust particle shape is assumed in each profile as indicated in the legend. The approx. aspect ratio is written on each particle.

The backscatter coefficient β, normalized by β at λ = 355 nm and dz = 1000 m, is shown in Fig. 4c. It decreases with ~~increasing height~~decreasing dz; e.g. at dz = 100 m and the three lidar wavelengths, β of the reference ensemble is reduced by 41 %, 49 %, and 63 %, respectively, compared to β at dz = 1000 m.

The extinction coefficient α (Fig. 4d) also decreases towards the SAL top; the relative decrease, however, is smaller than for β, e.g. for the reference ensemble we find values of 36 %, 40 %, and 50 % for the height levels mentioned above. WASO particles influence the wavelength dependence of β and α at any dz.

In the following we focus on δ_l at λ = 532 nm because δ_l is the intensive aerosol property, i.e. not depending on the amount of particles, which can be measured with high vertical resolution (compared to S from Raman lidar) and many depolarization lidar systems operate at this wavelength.

3.2 Sensitivity of δ_l profiles to particle shape

The shape mixture in our reference ensemble may not be fully representative for desert aerosol. Therefore, it is worthwhile to estimate the sensitivity of the lidar profiles to particle shape. ~~We focus on δ_l at λ = 532 nm because δ_l is most sensitive to particle shape and many depolarization lidar systems operate at this wavelength.~~

Fig. 5 shows δ_l profiles at λ = 532 nm for [H1, 5 d] where all dust particles of the reference ensemble were replaced by particles of only a single shape, as indicated in the legend together with their approx. aspect ratios. The other microphysical properties of the dust particles and the properties of the spherical WASO particles were left unchanged. For each profile, the shape-specific ξ_{vc}, as given above, is considered in the calculations.

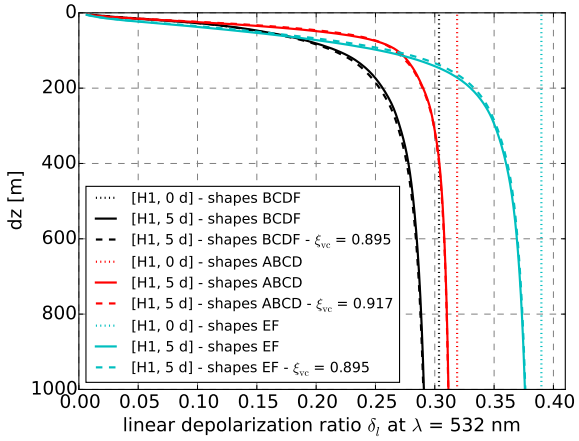

Figure 6. Analogous to Fig. 5, but assuming mixtures of different shapes of mineral dust particles as indicated in the legend (shapes BCDF = reference ensemble). The solid lines show profiles for [H1, 5 d]. The dashed lines show the same profiles when no shape dependence of the settling velocity is assumed (ξ_{vc} of all shapes is set to the average value, which is given in the legend). The dotted lines show the modeled profile at the beginning of the settling.

The absolute value of δ_l at $\lambda = 532$ nm depends on particle shape with a variation range from about 0.2 to 0.4 at $dz = 1000$ m. δ_l of elongated shapes (~~B,~~ C, F) tends to be smaller than δ_l of the more compact ~~shapes~~ counterparts (A, E)~~. The smaller-scale features in the profiles shown in Fig. 5 are a result of the variability of~~ , illustrating that there is no direct correlation between large aspect ratios and large δ_l ~~as function of size (see Fig. 2 of Gasteiger et al. (2011) where the single particle properties are shown~~(in contrast to what is often assumed in the literature). δ_l decreases with ~~height~~ decreasing dz for all considered shapes ~~. The~~ and the decrease is not strongly sensitive to the selection of the particle shape. However, the decrease of δ_l in case of shapes D-F (aggregate particles, edged particles) tends to be shifted to ~~lower altitudes~~ larger dz compared to δ_l in case of ~~the other shapes~~ shapes A-C (deformed spheroids). The sensitivity of δ_l profiles to realistic changes of the refractive index and the size distribution was found to be lower (not shown) than the sensitivity to the particle shape (Fig. 5).

3.3 Sensitivity of δ_l profiles to shape dependence of settling velocity

~~As the next step we investigate the importance of~~ Yang et al. (2013) suggest a model for settling-induced separation of particle shapes to explain the observed height dependence of δ_l. They consider the shape dependence of the ~~gravitational settling for~~ settling velocity v but not the size dependence of v. Here, we investigate how sensitive δ_l profiles ~~. For this investigation at least two different dust particle shapes need to be mixed within the model ensembles.~~ are to the shape dependence of v compared to the size dependence of v. For this purpose, Fig. 6 shows δ_l profiles at $\lambda = 532$ nm for [H1, 5 d] and for three different shape mixtures, which are indicated by color (mixture BCDF corresponds to the reference ensemble used in most other parts of this paper). The solid lines illustrate results when shape-dependent ξ_{vc} are considered. By contrast, results shown as dashed

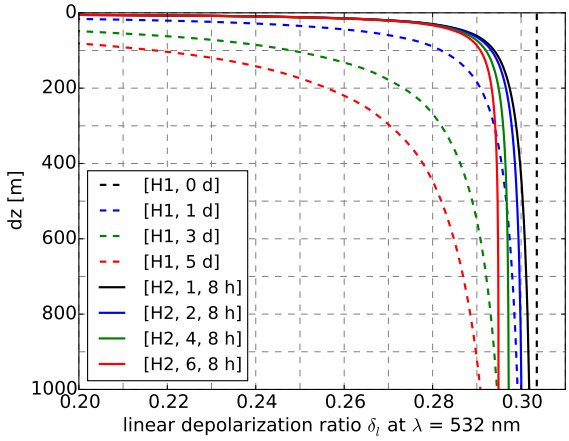

Figure 7. Linear depolarization ratio δ_l profiles at $\lambda = 532$ nm in the upper 1 km of the SAL for both hypotheses after different transport time periods.

lines assumed ~~an~~ the average ξ_{vc} value (as ~~indicated~~ displayed in the legend) for the settling of all dust shapes, implying that the ~~settling velocity~~ shape dependence of v ~~varies within the specific ensembles only as function of r_c~~ is switched off. For comparison also the initial δ_l profiles ~~(~~at [H1, 0 d] ~~)~~ are shown as dotted lines. Thus, the differences between the dotted and the solid ~~profiles~~ lines show the total settling effect after 5 days without ~~convective~~ vertical mixing and the differences between solid and dashed lines show the effect ~~that result from~~ of the shape dependence of the settling velocity. The latter effect is much smaller than the total settling effect, ~~which~~ independent of the assumed shape mixture. This allows us to conclude that the ~~shape dependence of the settling velocity~~ settling-induced separation of particle shapes is only of minor importance for δ_l compared to the ~~size dependence~~settling-induced separation of particle sizes. These results are consistent with results presented by Ginoux (2003)~~, but deviate from the model applied by Yang et al. (2013)~~.

3.4 Effect of diurnal convection cycle (H2)

Figure 7 shows δ_l profiles for both hypotheses, different time periods without ~~convection~~ mixing (t_s), and different number of nights (i_{night}), assuming our reference ensemble as the initial ensemble. The effect of settling on the δ_l profile increases with increasing ~~convection-free time~~t_s, in particular in the upper few hundred meters of the SAL (H1, compare dashed lines). In case day-time convective mixing occurs (H2), the night-time δ_l profile (shown here for ~~t_s = 8 h, i.e.~~ 8 hours after sunset) changes only slightly from day to day, with the maximum changes occurring at lower altitudes (compare solid lines). For example, δ_l is reduced by about 0.007 at dz = 1000 m from the first night (i_{night} = 1) to the sixth night (i_{night} = 6). The ~~difference of~~ differences between the δ_l profiles ~~between~~ for H1 and those for H2 ~~increases~~ increase with time (~~compare~~ lines of same color correspond to approx. the same transport time), illustrating the sensitivity of the δ_l profiles to the occurrence of ~~convective~~ vertical mixing.

4 Comparison with SALTRACE data~~: Case study 11 July 2013~~

We now discuss our modeling results based on a comparison with ~~SAL~~ aerosol data measured during the SALTRACE field campaign ~~on 11 July 2013. In this and the subsequent section, we~~ (Weinzierl et al., 2016) in the upper 1 km of the SAL and test our two hypotheses using this data set.

4.1 Lidar measurements

Lidar measurements and radiosonde launches were performed on the grounds of the Caribbean Institute for Meteorology and Hydrology in Bridgetown, Barbados (13.15° N, 59.62° W, 110 m above sea level). Data ~~at λ = 355 nm and 532 nm~~ from the lidar system POLIS of the LMU (Munich) ~~(Freudenthaler et al., 2016; Groß et al., 2015)~~ (Groß et al., 2015; Freudenthaler et al., 2016) , data from the lidar system BERTHA of the TROPOS (Leipzig) (Althausen et al., 2000; Haarig et al., 2016, 2017) , and radiosonde data measured by TROPOS ~~(Leipzig)~~ are available. POLIS ~~is a Raman lidar~~ and BERTHA are Raman lidar systems, thus requiring strong temporal and vertical smoothing for the determination of profiles of lidar ratio S and extinction coefficient α. A vertical smoothing length of at least 500 m is required for those properties, but even with this smoothing length the signal-to-noise ratio of the Raman measurements is still too low for a meaningful comparison with our modeled vertical profiles. Therefore, we restrict our comparison to the linear depolarization ratio δ_l and the backscatter coefficient β, ~~which are also available from POLIS and require a smoothing length of about 180 m~~for which a significantly shorter smoothing length is sufficient. Furthermore, we consider only λ = 532 nm for our comparison~~because this wavelength is more sensitive to particle settling effects than λ = 355 nm (see Fig. 4)~~.

The lidar measurements presented in this section were performed around ~~0-1 UTC on~~ 0 UTC in the night from 10 to 11 July ~~2013, which is about 2 h after sunset~~2013. Sunset was at 22:28 UTC. Back trajectory analysis for this air mass using HYSPLIT (Draxler and Rolph, 2015) suggests that it had left the African continent about 5 days before the measurements (~~not shown). Thus, to~~ see supplement S-2). To test our hypotheses about the occurrence of ~~convective~~ vertical mixing, we assume for this comparison t_s = ~~2 h and $i_{\mathrm{night}} = 6$~~ 5 d in case of ~~H2~~H1, and t_s = ~~5 d~~ 2 h and $i_{\mathrm{night}} = 6$ in case of ~~H1~~H2.

Fig. 8~~illustrates measured and modeled vertical profiles. Fig. 8~~a shows radiosonde data of water vapour mixing ratio (~~magenta~~blue) and potential temperature (black). The potential temperature is nearly constant within the SAL, which extends up to about 4600 m above ground. This potential temperature profile indicates that ~~convection could~~ vertical mixing might have occurred during the transport of this air mass over the Atlantic. The relative humidity ~~in~~ at 4500 - 4600 m is about 50 % to 54 %. The vertical structure of the water vapour mixing ratio and the potential temperature might be regarded as typical for the Saharan Air Layer (Carlson and Prospero, 1972).

Fig. 8b ~~contains measured particle backscatter coefficients~~ and Fig. 8c show β and δ_l profiles measured by POLIS (black line), temporally averaged over almost 1 hour, including the sum of the systematic and statistical uncertainties. Fig. 8d and Fig. 8e show β and δ_l profiles measured by BERTHA (black line), ~~as well as profiles calculated~~ temporally averaged over 1.5 hours, including the estimated uncertainties. For comparison, also profiles modeled for our hypotheses H1 (red) and H2 (green) ~~. The amount of particles in the model was scaled to match the measured β close to the top of the SAL.~~ are plotted in Fig. 8~~c~~

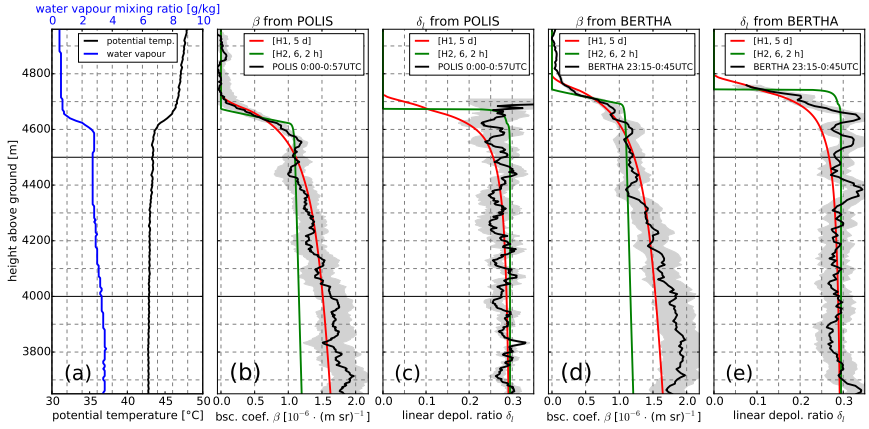

Figure 8. Vertical profiles over Barbados around 0 UTC on 11 July 2013. (a) Profile of potential temperature (black) and water vapour mixing ratio (~~magenta~~blue) from a radiosonde launched at 23:39 UTC on 10 July 2013. (b) Particle backscatter ~~coefficients~~ coefficient β ~~at λ = 532 nm.~~ and (c) ~~Particle~~ particle linear depolarization ~~ratios~~ ratio δ_l at λ = 532 nm ~~. Both β and δ_l measured with~~ from POLIS measured between 0:00 UTC and 0:57 UTC on 11 July 2013. (~~black~~d) Particle backscatter coefficient β and (e) particle linear depolarization ratio δ_l at λ = 532 nm from BERTHA measured between 23:15 UTC on 10 July 2013 and 0:45 UTC on 11 July 2013. The shaded area indicate the sum of the systematical and statistical uncertainties of the measured profiles. Corresponding modeled lidar profiles ~~assuming a SAL top height of 4660 m, as well as~~ for H1 (red) and H2 (green) are shown. ~~For H1 also a profile for a~~ The SAL top ~~height~~ heights of ~~4740 m is plotted~~ the modeled profiles were fitted to the measured β profiles (~~thin red lines~~heights given in main text). A flat smoothing window of ~~180~~ about 50 m is used for the measured and modeled lidar profiles.

~~shows corresponding measured and modeled δ_l profiles. The top of~~ . The SAL top heights of the modeled profiles were fitted to the ~~SAL was set to 4660 m in the modeled profiles. For H1, 5 dwe considered, in addition, a case with the~~ measured β profiles. The fitted SAL top height ~~set to 4740 m which better matches the lidar measurements (thin red line)~~is 4700 m for H1 and 4650 m for H2 in case of POLIS, whereas it is 4770 m for H1 and 4720 m for H2 in case of BERTHA. Measured and modeled lidar profiles shown in Fig. 8 were vertically smoothed with a flat window of about ~~180~~ 50 m length.

~~Modelled and~~ The measured β ~~agree fairly well near the SAL top if~~ profiles are better fitted by the profile modeled for H1 than by the profile modeled for H2 ~~, 6, 2his assumed~~ (Fig. 8b ~~). The slope of β near the SAL top is mainly determined by the smoothing length applied. Below 4400 m the measured β is larger than the modeled one, which hints to inhomogeneities in the spatial aerosol distributions not considered in our model.In case of H1, 5 d(thick red line) deviations from β measurements are large, but they are reduced if the SAL top height is 4740 m (thin red line). This shift in top height reduces the consistency with the radiosonde data; we cannot exclude that such differences in SAL top height between radiosonde and lidar measurements are real, but we have no further evidence for that.~~

and Fig. 8d). The modeled δ_l ~~in the SAL is generally larger than~~ for H1 and H2 is generally close to the measured δ_l in the lower part of the SAL (Fig. 8c ~~), which may be due to the natural variability between different aerosol source regions. While~~

assuming H2 (green) better captures the measured steep decrease near the SALtop, assuming and 8e). At the top of the SAL, where the measurement uncertainties are considerable, the measured δ_l profiles deviate from each other and no conclusion on whether H1 with a higher SAL top height than found in the radiosonde data (thin red line) somewhat better captures the shape of the or H2 better explains the δ_l profile in the upper 1 km. If we assume that the SAL top height shift between lidar and radiosonde could be real, we can conclude that both hypotheses roughly explain the measurements and that uncertainties in our model and the measurements do not allow us to determine which of our hypotheses fits better. However, if we assume that profiles can be drawn. At other days during SALTRACE, the SAL top height did not vary that strong between radiosonde and lidar measurements, H2 (convection over Atlantic) fits better than H1 (no convection)lidar profiles and their uncertainties exhibit similar characteristics in the SAL (not shown). Our comparisons indicate that further reductions of uncertainties are desirable to identify transport effects within the SAL by means of lidar data. The investigation of profiles at other wavelengths, e.g. δ_l at λ = 1064 nm (Haarig et al., 2017) , might also bring further insights.

4.2 Optical particle counter measurements

During SALTRACE, the optical particle counter instrument CAS-DPOL (Cloud and Aerosol Spectrometer with Depolarization Detection (CAS-DPOL manufactured by DMT, Boulder, CO, USA) was operated under the wings of the Falcon aircraft DLR research aircraft Falcon. The ambient air flows passively through the instrumentthis optical particle counter. It has a laser as light source operating at λ = 658 nm and measures the intensity of light scattered forward to 4°-12° by individual particles flying through its sampling area. Each particle is counted and from the measured intensity its size is inverted. The counts are collected in 30 size bins, covering a nominal radius range from 0.25 µm to 25 µm. From these counts, and knowing the true airspeed of the aircraft These size bins and the size of the sampling area, the ambient particle number concentration N is calculated for each size bin. Thereby, the CAS-DPOL provides calibration used here were provided by the manufacturer of the instrument. The size-resolved in-situ measurements of the coarse mode size distribution allowing data from CAS-DPOL allows us to test more directly the size distributions resulting from our hypotheses maximum cut-off radius calculated in case of H1and H2.

For this test we use data from a flight flights performed during day-time on 22 June 2013, 10 July 2013, and 11 July 2013. Using the nominal size bins provided by the manufacturer of the instrument, the data was grouped in size ranges that are affected differently by particle settling . The aircraft position, at the time when the data used here was measured, is illustrated in Fig. S-3 (supplement). To extract the information about settling-induced separation of sizes, we use size bins for which we would expect no counts at low dz due to settling in case of H1 and normalize them by counts measured with the same instrument in a size range that is almost not affected by settling (Fig. 1). The results are illustrated in Fig. 9shows ratios of number concentrations N: The blue graph shows the ratio between N in the range r = 2.0 to 4.0 and N in the range . The blue lines show the counts in the nominal size bin r = 0.5 to 2.0 2.5 µm (size bin no. 17), whereas the green line shows the ratio between N in the range lines show the counts in the nominal size bin r = 2.5 to 7.5 3.25 µm and N in the range (size bin no. 18), both normalized by the counts in the size bins from r = 0.5 0.32 µm to 2.0 0.59 µm . Because of the strong decrease of dN/dr with increasing size of coarse particles, N in these size ranges is mainly determined by dN/dr at the lower boundaries of

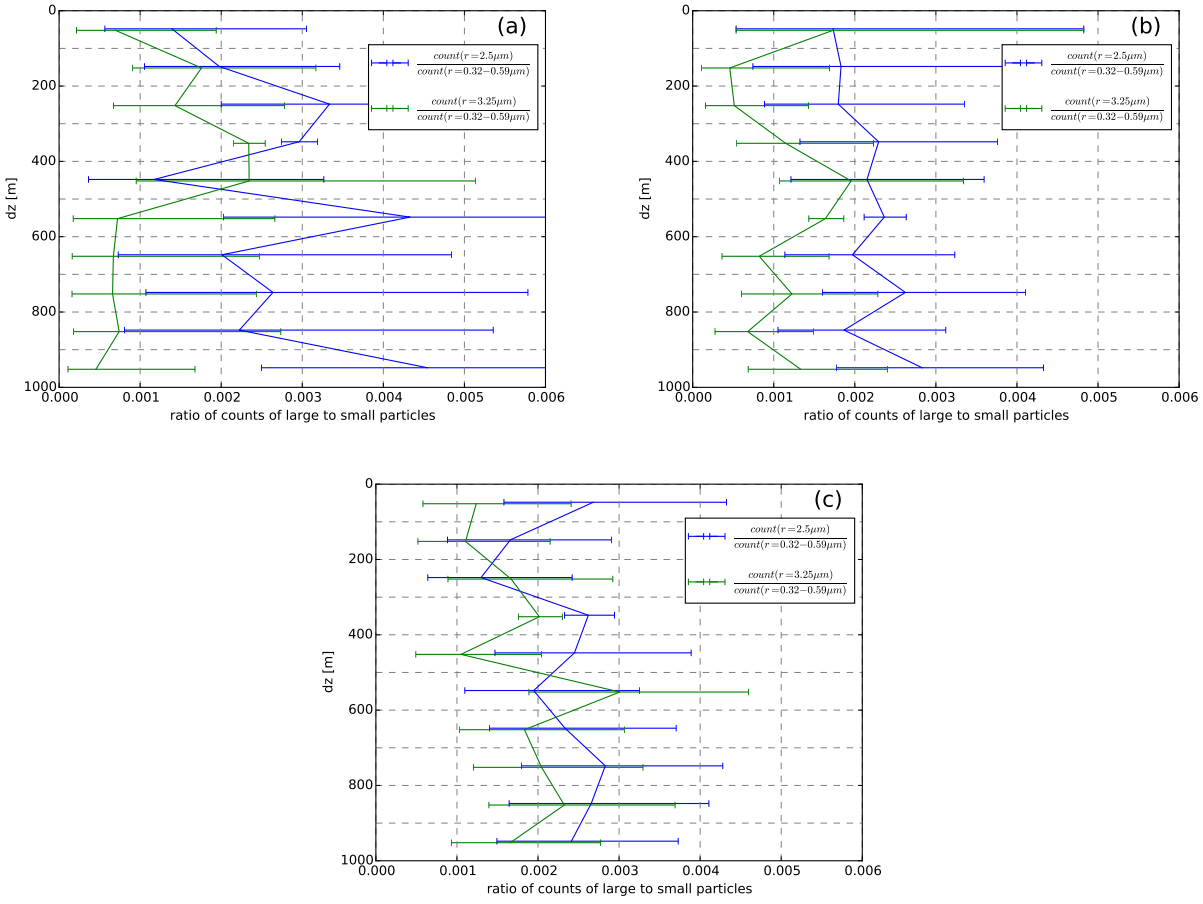

Figure 9. Ratios between ~~number concentrations *N*~~ counts in different ~~radius~~ size ranges measured by CAS-DPOL during ~~Falcon~~ aircraft ascent and descent (a) between ~~12~~ 18:09 and 20:10 UTC on 22 June 2013, (b) between 15:14 and 16:42 UTC on ~~11~~ 10 July 2013~~close to Barbados~~ , and (~~day-time~~c) between 12:45 and 13:50 UTC on 11 July 2013. The aircraft locations are illustrated in Fig. S-3 (supplement). The vertical axis shows the distance from the SAL top. The data was grouped in 100 m wide vertical bins. The error-bars are Poisson 95 % confidence intervals.

(size bin no. 2-9). Analysis of calibration measurements performed during SALTRACE suggests that the sizes presented here are underestimated because the instrument optics was polluted by dust particles which reduced the amount of light reaching the detector (the optics was not polluted during the calibration by the ranges. Therefore, the plotted ratios basically are ratios between the number of coarse particles (potentially affected by particle settling) and the number of smaller particles (hardly affected by particle settling). manufacturer).

The in-situ data is available at one second resolution, which corresponds to about 8 m vertical resolution during ascent and descent of the investigated flightflights. Because of the low number of counts per second for $r \geq 2.0$ coarse particles, we grouped the data in 100 m wide vertical bins. The vertical bins are described by their distance dz from the SAL top , with the SAL top as determined from the CAS-DPOL data. The SAL top was at 3700 m asl both during ascent and descent on 22 June, at 5050 m during ascent and at 4900 m during descent on 10 July, and at 4630 m asl during ascent and at 4550 m asl during descent as determined from the CAS-DPOL data. on 11 July 2013. Each dz bin covers about 25 seconds of data, except the bin from dz = 300 m to 400 m, which covers about 500 seconds of data because the bins in which the ascent or descent was paused flying at constant altitudefor several minutes. As a result of the vertical binning, the number of detected particles with r = 2.5 to 7.5 is increased to 14 - 24 in each bin at $dz \geq 400$ m.

As illustrated in Fig. 1, we expect in case of our first hypothesis (H1) that particles larger than with $r \approx 2.5$ µm and larger are removed from $dz <$ 600 550 m after 5 days over the Atlantic. However, the green line curves in Fig. 9 shows show that such particles are detected also in the upper 100 m of the SAL near Barbados. This indicates H1 to be unrealistic even if intrinsic uncertainties of the size determination by CAS-DPOL on the order of ±50 % are assumed. In case of H2, we assume that the SAL is well-mixed and thus the aerosol profiles are expected to be height-independent during day-time. Though a reduction of the fraction of large particles towards the SAL top is indicated in the measured in-situ profiles (Fig. 9), H2 agrees much better with the in-situ data than H1, suggesting A similar height dependence was found also during the PRIDE campaign which was based on Puerto Rico (Reid et al., 2003) . This suggests that some processes within the SAL keeps keep large particles longer in the air than expected from gravitational settling.

5 Comparison with average δ_l profiles from POLIS and CALIOP

After presenting the SALTRACE case study SALTRACE case studies in the previous section, we now use averaged lidar profiles to CALIOP δ_l profiles to get a more general view on the modification of the aerosols during the transport over the Atlantic and to test our hypotheses. Therefore We note that in reality the SAL transport is much more complex than our hypotheses assume and varies from case to case. Nonetheless, we expect that averaged profiles of the intensive property δ_l contains evidence about whether the occurrence of vertical mixing within the SAL is typical or not. In the following, we first describe how we average the POLIS and CALIOP δ_l dataand calculate the average δ_l from the CALIOP data, then compare our modeling results to these the averaged profiles in the upper 1 km of the SAL.

5.1 Averaging POLIS data

We consider the average δ_l profile at $\lambda = 532$ nm from POLIS during the SALTRACE measurement period from 20 June 2013 to 13 July 2013 at Barbados to get a more robust characterization of SAL profiles after long-range transport. The measurements used for averaging were performed during day and night. Sequences where SAL aerosol was measured were selected by visual inspection of the β, and δ_l profiles. 27 measurement sequences covering about 32 hours were considered for averaging. Only few sequences were performed in the hours before sunrise and around noon time. For the evaluation of the lidar data used in this section, a flat smoothing window of about 40 m and a height-independent lidar ratio of 55 sr is applied to the measurements. Averaging was performed relative to the SAL top, which was localized for each sequence also by visual inspection of the profiles. The average depolarization ratio was calculated from the summed up backscatter coefficients that had been separated into their parallel and perpendicular componentsfinally discuss our findings.

5.1 Averaging CALIOP data

To get a more general view on the optical properties of the aerosols at the top of the SAL during the transport from Africa over the Atlantic we evaluate measurements of the CALIOP lidar.

We restrict our analysis again to δ_l at 532 nm as because this parameter is relatively insensitive to errors encountered in the extinction-backscatter retrieval (Liu et al., 2013), which may result, e.g. from uncertainties in the lidar ratio (Wandinger et al., 2010; Amiridis et al., 2013). We again analyze the upper 1 km of the SAL, where potential settling effects would and mixing effects should be observable with lidar (Fig. 7). We use CALIPSO level 2 aerosol profile products v3.01 (NASA, 2010) of backscatter coefficients β and the perpendicular components of the backscatter coefficients $\beta_\perp$ at $\lambda = 532$ nm measured during summer 2007-2011, i.e. from June to August of each of the five years. We excluded profiles measured on 23 June 2009 and on 2 Aug 2009 because of unrealistic large measurement uncertainties found on that dayoutliers found in the data from these days. Powell et al. (2009) describe how backscattering quantities are calculated from the CALIOP raw data. Vaughan et al. (2009) show the automated procedure to detect aerosol and cloud layers from using these backscattering quantities, and Liu et al. (2009) demonstrate how aerosols are discriminated from clouds. We restrict our evaluation to night-time measurements in the region from 10°N to 30°N and 0°W to 8075°W. We group these measurements in four three longitude ranges of 2025° width along the transport path from Africa to the Western Atlantic. All Only night-time measurements are considered; all measurements were performed approximately 8 h after sunset.

The CALIOP measurements are performed with a vertical resolution of 30 m and a horizontal resolution of 330 m. The backscatter coefficients β and $\beta_\perp$ are provided in the level 2 data with a vertical resolution of 60 m (i.e. for bins of 60 m height) and a horizontal resolution of 5 km, which reduces the noise compared to the measured resolution. As discussed by Vaughan et al. (2009), aerosol features are detected with 30 m vertical resolution using an iterative procedure starting with the horizontal resolution of 5 km. As the noise can be considerable at 5 km resolution, in particular if particle concentrations are low, the horizontal resolution is subsequently increased to 20 km and 80 km to detect also weaker features. Depending on the results of the feature detection, the backscatter coefficients are horizontally averaged over 5 km, 20 km, or 80 km, and the horizontal averaging range can depend on height. In the following we use only data horizontally averaged over 5 km.

From the large set of aerosol profiles, the profiles that fulfill the following criteria are selected for averaging:

- Uppermost aerosol-containing bin between 3 and 8 km above sea level
- Both sub-bins (30 m ~~resolution~~height each) of uppermost aerosol-containing bin classified as aerosol-containing
- All 16 bins (i.e. up to ≈1 km) below uppermost aerosol-containing bin also classified as aerosol-containing
- No cloud-containing bin detected in or above 17 uppermost aerosol-containing bins
- Data horizontally averaged over 5 km (not 20 or 80 km) in each of the 17 uppermost aerosol-containing bins
- Linear depolarization ratio δ_l, averaged over 17 uppermost aerosol-containing bins, larger than 0.10

~~After the selection of profiles,~~ β and $\beta_\perp$ of each of the 17 vertical bins is summed up over all selected profiles. From these sums, the average δ_l for each bin is calculated according to

$$\delta_l = \frac{\beta_\perp}{\beta - \beta_\perp} \frac{\sum \beta_\perp}{\sum \beta - \sum \beta_\perp}. \tag{9}$$

The measurement uncertainties ~~of β and $\beta_\perp$~~ $\Delta\beta$ and $\Delta\beta_\perp$ provided in the CALIOP profile data are ~~assumed to be random and uncorrelated (Young, 2010) . They are~~ based on a simplified analysis assuming that all the uncertainties are random, uncorrelated and produce no biases (Young, 2010) . The magnitude of the uncertainties is mainly determined by the signal-to-noise ratio (Hunt et al., 2009). To calculate the estimated statistical uncertainty $\Delta\delta_l$ of the average δ_l value for each bin (Eq. 9), we sum up the squares of the measurement uncertainties of each profile and use

$$\Delta\delta_l = \frac{\sqrt{\left(\sum \beta\right)^2 \cdot \sum \left(\Delta\beta_\perp\right)^2 + \left(\sum \beta_\perp\right)^2 \cdot \sum \left(\Delta\beta\right)^2}}{\left(\sum \beta - \sum \beta_\perp\right)^2}. \tag{10}$$

As we average over a large number of profiles, the ~~relative~~ uncertainties of the averaged profiles are reduced considerably compared to the uncertainties of single profiles.

5.2 Comparison with averaged profiles

~~The averaged linear depolarization ratio profile from POLIS decreases slightly with increasing altitude from about 0.28 at dz = 1 km to about 0.27 at dz = 100 m and to about 0.25-0.26 for dz < 100 m (see orange line in Fig. 10). No significant differences in the average profiles were found between day-time and night-time data (not shown).~~

Figure 10 shows ~~also~~ the averaged δ_l profiles calculated from the CALIOP profile data considering all profiles that fulfilled the above-mentioned criteria. The averaged data of the uppermost bin is plotted at $dz \approx 30$ m, the subsequent bin at $dz \approx 90$ m, etc. While the ~~dark blue~~ blue solid line shows the average δ_l close to the aerosol source region, the distance from the source region increases ~~for the green , red, and light blue lines. The light blue line shows the average from a region mainly covering the Caribbean~~with the green line (Central Atlantic) and red line (Western Atlantic). A map illustrating these regions is provided in the supplement S-4. Averages were taken over ~~7623, 7502, 5459, and 1738~~ 9061, 9114, and 3846 individual profiles in the

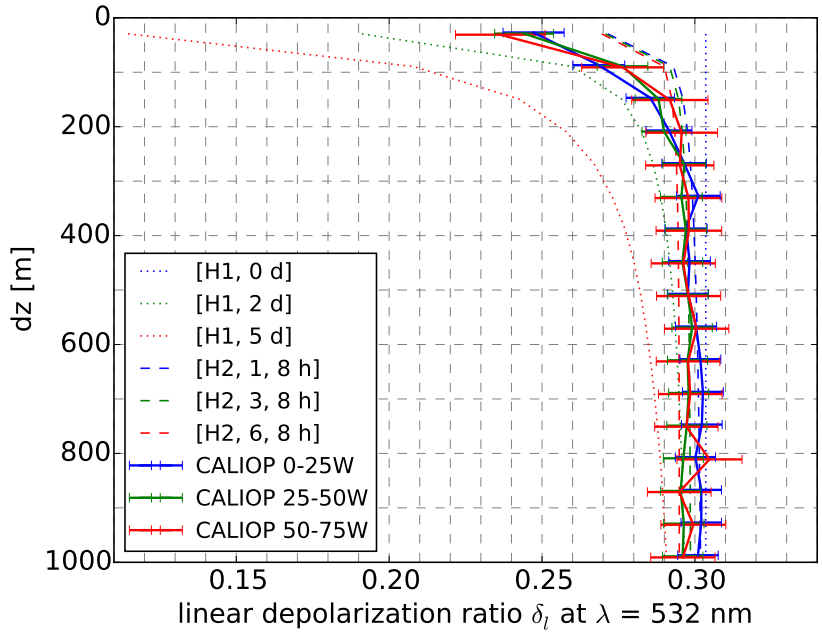

Figure 10. Linear depolarization ratio δ_l profiles at $\lambda = 532$ nm in the upper 1 km of the SAL. ~~The average profile measured by POLIS during SALTRACE in Barbados is shown as the orange line.~~ CALIOP profiles averaged over profiles from summer months 2007-2011 that fulfill conditions listed in the text are shown as ~~dark~~ blue, green, ~~red,~~ and ~~light blue~~ red solid lines. ~~These~~ The colors denote different longitude ranges. Error bars of the CALIOP profiles show the estimated statistical uncertainty $\Delta\delta_l$ of the ~~mean~~average δ_l. For comparison also model results for ~~different setups~~ both hypotheses are shown as ~~black~~ dotted (H1) and dashed (H2) lines. ~~A flat smoothing window of 60 m is used for the modeled lidar profiles.~~

~~4~~ 3 respective regions along the SAL transport path. Considering the statistical uncertainty of the ~~mean, the mean~~ average, the average δ_l does not vary along the SAL transport path and is height-independent with values close to 0.30 for $dz > 250$ m. δ_l decreases towards the SAL top to values of about 0.23~~-0.26~~ -0.25 in the uppermost bin.

~~There are some deviations between the averaged profile from POLIS and from CALIOP (Fig. 10). These deviations can be a result of the natural variability of the desert aerosol properties in combination with the differences in the temporal and spatial coverage of these data sets. In addition, the assumptions made about the lidar ratio potentially affect the POLIS data shown in Fig. 10.~~

Comparing the measured with the modeled profiles, it becomes clear that the strong decrease of δ_l in the upper 100 m of the SAL, as modeled for long-range transport without ~~convective~~ vertical mixing (H1, ~~black~~ red dotted line), is ~~found neither in the averaged POLIS data nor~~ not found in the averaged CALIOP data over the Western Atlantic (~~orange, red , and light blue lines~~red solid line). This indicates our first hypothesis (H1) to be unrealistic. A further result that renders H1 unlikely is the

fact that the average δ_l profile from CALIOP is not modified during transport while one would expect significant changes of the δ_l profile during transport if H1 is assumed (~~see dashed lines in Fig. 7~~compare the dotted lines of different colors).

The ~~black solid and the~~ dashed lines in Fig. 10 show the δ_l profile when ~~convective~~ day-time convective vertical mixing is assumed (H2). These modeled δ_l profiles are relatively height-independent, except in the upper 100 m of the SAL. ~~Comparing the POLIS measurements, which were averaged over day-time and night-time, with these profiles shows a fairly good agreement in profile shape, but an almost height-independent difference of about 0.01 to 0.02. Despite this difference, this comparison with POLIS data suggests~~ Fig. 10 shows that considering vertical mixing (using H2 ~~to be much more realistic than H1.Comparison of the CALIOP profiles with our modeling results also suggests that considering convective mixing (~~instead of H1) reduces considerably the deviation of the model from the measurements after long range transport. Also the invariability of the average δ_l profile between the different regions is much better captured if H2 ~~) is required to explain the measured data sets.~~

is assumed. Our model for H2 predicts a reduction of δ_l by about 0.007 at dz = 1 km after about 5 days (~~Fig. 7~~see dashed lines). This reduction ~~in~~ is not seen in the CALIOP profiles, possibly because it is within the range of the statistical uncertainty of the averaged δ_l profiles from CALIOP~~(Fig. 10)~~.

5.3 Discussion of comparison ~~between H2 and CALIOP~~ with averaged profiles

Our model assuming day-time convection (H2) ~~agrees well with~~ explains the averaged CALIOP data and its invariability between the regions for the most part. However, deviations of the δ_l profile between this model and the averaged CALIOP data occur in the upper 2-3 bins (compare dashed to solid lines in Fig. 10). The measurements indicate on average a stronger removal of large particles ~~near the SAL top~~ in the upper 100 m of the SAL over Africa and over the Atlantic than ~~our model for~~ H2 suggests~~(solid and dashed black lines). There are several potential reasons for deviations: In our model we~~ . We again emphasize that we average over a large number of different cases. The δ_l profiles may vary from case to case, which however is hard to quantify from the CALIOP data because of large statistical uncertainties of single profiles.

One source of deviation could be our settling and vertical mixing model in H2. We assume perfect mixing of particles over the complete SAL when convection occurs and we assume a sharp boundary between the SAL and the layer above. But it ~~is~~ might be plausible that some mixing occurs between the SAL and the layer above on the order of 10 m to 100 m. Thus, some ~~desert~~ Saharan aerosol near the upper boundary of the SAL might ~~be~~ become decoupled from the ~~day-time convection~~ mixing within the SAL, allowing there a stronger removal of large particles than ~~our model~~ H2 predicts. However, one fact that contradicts these considerations is that the measured δ_l profile seems to be independent of ~~transport time (compare CALIOP profiles in Fig. 10)~~ region while one would expect that such effects become larger with ~~transport time~~distance from the source regions.

Another source of uncertainty is related to our aerosol model. Natural desert aerosol has very complex microphysical properties (e.g. Kandler et al., 2011) , and as a consequence, our model of the Saharan aerosol mixtures contains several assumptions and the calculated optical properties are connected with uncertainties. Though we argue that our model mixture represents lidar-relevant optical properties of Saharan aerosols well (Gasteiger et al., 2011) , we can not exclude that the

deviations of the modeled δ_l profiles (H2) from the averaged measurements in the upper 2-3 bins are related to assumptions in our aerosol mixture and the optical modeling approach.

A further aspect that ~~has~~ needs to be kept in mind is that multiple scattering could affect the CALIOP measurements (Wandinger et al., 2010). In case of our SAL top study, the multiple scattering effect would increase with increasing dz as the lidar pulse penetrates the SAL from its top. It is well-known that with increasing amount of particles the multiple scattering effect increases (e.g. Bissonnette et al., 1995). Using the CALIOP profile data we do not find a significant dependence of the δ_l profiles on the absolute values of β (not shown), indicating that multiple scattering does not significantly affect the averaged δ_l profiles.

To investigate the CALIOP profiles in more detail, an analysis is provided in the supplement S-4, considering also 20 km and 80 km horizontal averages, the year-by-year variability, sub-bin classification~~(which is provided in the profile data at 30 m vertical resolution)~~, the cloud-aerosol discrimination, and the sensitivity to the δ_l threshold. The sensitivity of the averaged δ_l profile ~~shapes~~ to these parameters was found to be low. As a consequence, it seems likely that the simplifications in ~~our model~~H2 (including the optical model) are the reason for the remaining deviations near the SAL top. Also the average β profile (see supplement S-4), as well as the variability of the backscatter coefficient β from case to case (not shown), can not be explained using H2, showing the need to consider in future research further aspects for precise SAL transport modeling.

6 Summary and conclusions

Transport of aerosol in the Saharan Air Layer (SAL) over the Atlantic is relevant for weather and climate but important processes within the SAL still are not well understood. To gain insights in relevant processes, we developed a model which describes the modification of the vertical aerosol distribution in the upper 1 km of the SAL during transport based on the physical processes of gravitational settling and ~~convective~~ vertical mixing. From the vertical aerosol distributions, lidar profiles are calculated using explicit optical modeling. Sensitivity studies revealed (a) that generally the particle linear depolarization ratio decreases towards the SAL top for all considered model shapes, and (b) that the size dependence of the settling velocity is significantly more important for the linear depolarization ratio profile than ~~its shape dependence~~ the shape dependence of the settling velocity.

The model results were compared to lidar and in-situ measurements and two hypotheses about the occurrence of ~~convective~~ vertical mixing within the SAL were tested (H1 without mixing, H2 with convective mixing during the day). Comparisons with ground-based depolarization lidar measurements in Barbados, performed in the frame of the SALTRACE campaign, ~~indicate that it is very likely that convective~~ revealed that the measurement uncertainties are in the same order as the differences between both hypotheses. Vertically resolved in-situ measurements of the size distribution during SALTRACE found large particles in the upper part of the SAL that are not consistent with H1, indicating that vertical mixing occurs in the SAL over the Atlantic. These findings are ~~strongly supported by~~ supported by results from an analysis using night-time ~~depolarization profiles~~ data from CALIOP. ~~Furthermore, the~~ The CALIOP data shows that the average linear depolarization ratio profile in the upper 1 km of the SAL does not change along its transport path over the Atlantic~~. Our comparisons~~

lead us to the conclusion that the size distributions, at least in the range $r <\approx$ 3-5 , are hardly modified during transport after the first night after mobilization, which disproves H1. These findings are consistent with results from other studies about Saharan aerosol which found that the aerosol properties do not change significantly during long-range transport, e.g. Reid et al. (2003); Maring et al. (2003); Weinzierl et al. (2011); Mahowald et al. (2014); Denjean et al. (2016a); Weinzierl et al. (2016) Re

Our We could show that vertical mixing occurs within the SAL and our model assuming day-time convective mixing (H2), which is driven by the idea that the Saharan aerosol absorbs sunlight triggering convection, explains the CALIOP most data quite well. Howeversome deviations remain that might originate from the simplifications of our , there are limitations of this idealized model. For example, we profiles of extensive properties like the backscatter coefficient often can not be explained with H2 and remaining deviations from the averaged CALIOP depolarization data are still unexplained. We did not consider the possibility of night-time convection, of weak convection (i.e. non-perfect vertical mixing)weak vertical mixing, of size-selective particle removal at the lower boundary of the SAL during convectionvertical mixing, or effects due to electrical fields in the SAL, which may occur in reality. In this connection, it needs to be investigated if heating by solar radiation during day-time is indeed the main driving force for convection. For example, also radiative . Radiative effects in the thermal infrared could might be an important aspect to consider for convective mixing understanding the vertical mixing in the SAL, as discussed by Carlson and Prospero (1972). Measurements of aerosol properties and vertical wind speeds with high vertical and temporal resolution using lidar in combination with airborne in-situ instruments, radiative transfer calculations, and convective models might help to deepen our understanding of processes affecting The development of turbulence due to vertical wind shear, more realistic air layer dynamics, and feedbacks of radiative effects with the dynamics (Chen et al., 2010) are possible further aspects to be considered for a precise understanding of the processes within the SAL, their variability, and their effect on size distributions and lifetime of super-micron particles.

Acknowledgements. The research leading to these results has received funding from LMU Munich's Institutional Strategy LMUexcellent within the framework of the German Excellence Initiative and from the European Research Council under the European Community's Horizon 2020 research and innovation framework program/ERC grant agreement No. 640458 - A-LIFE. S. Groß acknowledges funding by a DLR VO-R young investigator group. The SALTRACE campaign was mainly funded by the Helmholtz Association, DLR, LMU, and TROPOS. We thank the ground-based remote sensing group of the Leibniz-Institut fr Troposphrenforschung (TROPOS), led by Albert Ansmann, for providing radiosonde data. The Caribbean Institute for Meteorology and Hydrology in Bridgetown, Barbados kindly provided the infrastructure to perform the SALTRACE lidar measurements. The CALIOP data were obtained from the NASA Langley Research Center Atmospheric Science Data Center. We thank the reviewers of a previous version of this manuscript for are grateful to Volker Freudenthaler for fruitful discussions on our model and the lidar data. We thank all reviewers for their suggestions that helped us to substantially improve itour manuscript.

References

Althausen, D., Müller, D., Ansmann, A., Wandinger, U., Hube, H., Clauder, E., and Zörner, S.: Scanning 6-Wavelength 11-Channel Aerosol Lidar, J. Atmos. Oceanic Technol., 17, 1469–1482, doi:10.1175/1520-0426(2000)017<1469:SWCAL>2.0.CO;2, 2000.

Amiridis, V., Wandinger, U., Marinou, E., Giannakaki, E., Tsekeri, A., Basart, S., Kazadzis, S., Gkikas, A., Taylor, M., Baldasano, J., and Ansmann, A.: Optimizing CALIPSO Saharan dust retrievals, Atmos. Chem. Phys., 13, 12 089–12 106, doi:10.5194/acp-13-12089-2013, 2013.

Anderson, G. P., Clough, S. A., Kneizys, F. X., Chetwynd, J. H., and Shettle, E. P.: AFGL atmospheric constituent profiles (0-120km), Tech. rep., AFGL-TR-86-0110, Environemental Research papers No. 954, 1986.

Ansmann, A., Petzold, A., Kandler, K., Tegen, I., Wendisch, M., Müller, D., Weinzierl, B., Müller, T., and Heintzenberg, J.: Saharan Mineral Dust Experiments SAMUM-1 and SAMUM-2: What have we learned?, Tellus B, 63, 403–429, doi:10.1111/j.1600-0889.2011.00555.x, 2011.

Ben-Ami, Y., Koren, I., and Altaratz, O.: Patterns of North African dust transport over the Atlantic: winter vs. summer, based on CALIPSO first year data, Atmos. Chem. Phys., 9, 7867–7875, doi:10.5194/acp-9-7867-2009, 2009.

Bissonnette, L. R., Bruscaglioni, P., Ismaelli, A., Zaccanti, G., Cohen, A., Benayahu, Y., Kleiman, M., Egert, S., Flesia, C., Schwendimann, P., Starkov, A. V., Noormohammadian, M., Oppel, U. G., Winker, D. M., Zege, E. P., Katsev, I. L., and Polonsky, I. N.: LIDAR multiple scattering from clouds, Appl. Phys. B, 60, 355–362, doi:10.1007/BF01082271, 1995.

Carlson, T. N. and Prospero, J. M.: The large-scale movement of Saharan air outbreaks over the northern equatorial Atlantic, J. Appl. Meteor., 11, 283–297, doi:10.1175/1520-0450(1972)011<0283:TLSMOS>2.0.CO;2, 1972.

Chen, S.-H., Wang, S.-H., and Waylonis, M.: Modification of Saharan air layer and environmental shear over the eastern Atlantic Ocean by dust-radiation effects, J. Geophys. Res. Atmos., 115, D21 202, doi:10.1029/2010JD014158, 2010.

Clift, R., Grace, J. R., and Weber, M. E.: Bubbles, Drops, and Particles, Academic Press, 1978.

Cuesta, J., Marsham, J. H., Parker, D. J., and Flamant, C.: Dynamical mechanisms controlling the vertical redistribution of dust and the thermodynamic structure of the West Saharan atmospheric boundary layer during summer, Atmosph. Sci. Lett., 10, 34–42, doi:10.1002/asl.207, 2009.

Denjean, C., Cassola, F., Mazzino, A., Triquet, S., Chevaillier, S., Grand, N., Bourrianne, T., Momboisse, G., Sellegri, K., Schwarzenbock, A., Freney, E., Mallet, M., and Formenti, P.: Size distribution and optical properties of mineral dust aerosols transported in the western Mediterranean, Atmos. Chem. Phys., 16, 1081–1104, doi:10.5194/acp-16-1081-2016, 2016a.

Denjean, C., Formenti, P., Desboeufs, K., Chevaillier, S., Triquet, S., Maillé, M., Cazaunau, M., Laurent, B., Mayol-Bracero, O. L., Vallejo, P., Quiñones, M., Gutierrez-Molina, I. E., Cassola, F., Prati, P., Andrews, E., and Ogren, J.: Size distribution and optical properties of African mineral dust after intercontinental transport, J. Geophys. Res. Atmos., 121, 7117–7138, doi:10.1002/2016JD024783, 2016b.

Draxler, R. and Rolph, G.: HYSPLIT (HYbrid Single-Particle Lagrangian Integrated Trajectory) Model access via NOAA ARL READY Website (http://ready.arl.noaa.gov/HYSPLIT.php), NOAA Air Resources Laboratory, Silver Spring, MD, 2015.

Esselborn, M., Wirth, M., Fix, A., Weinzierl, B., Rasp, K., Tesche, M., and Petzold, A.: Spatial distribution and optical properties of Saharan dust observed by airborne high spectral resolution lidar during SAMUM 2006, Tellus B, 61, 131–143, doi:10.1111/j.1600-0889.2008.00394.x, 2009.

Freudenthaler, V., Seefeldner, M., Groß, S., and Wandinger, U.: Accuracy of linear depolarization ratios in clean air ranges measured with POLIS-6 at 355 and 532 nm, EPJ Web of Conferences, 119, 25 013, doi:10.1051/epjconf/201611925013, 2016.

Gasteiger, J., Wiegner, M., Groß, S., Freudenthaler, V., Toledano, C., Tesche, M., and Kandler, K.: Modeling lidar-relevant optical properties of complex mineral dust aerosols, Tellus B, 63, 725–741, doi:10.1111/j.1600-0889.2011.00559.x, 2011.

Ginoux, P.: Effects of nonsphericity on mineral dust modeling, J. Geophys. Res. Atmos., 108, 4052, doi:10.1029/2002JD002516, 2003.

Groß, S., Freudenthaler, V., Schepanski, K., Toledano, C., Schäfler, A., Ansmann, A., and Weinzierl, B.: Optical properties of long-range transported Saharan dust over Barbados as measured by dual-wavelength depolarization Raman lidar measurements, Atmos. Chem. Phys., 15, 11 067–11 080, doi:10.5194/acp-15-11067-2015, 2015.

Haarig, M., Althausen, D., Ansmann, A., Klepel, A., Baars, H., Engelmann, R., Groß, S., and Freudenthaler, V.: Measurement of the Linear Depolarization Ratio of Aged Dust at Three Wavelengths (355, 532 and 1064 nm) Simultaneously over Barbados, EPJ Web of Conferences, 119, 18 009, doi:10.1051/epjconf/201611918009, 2016.

Haarig, M., Althausen, D., Ansmann, A., Engelmann, R., Baars, H., Klepel, A., Groß, S., Freudenthaler, V., Burton, S. P., Marinou, E., and Gasteiger, J.: Triple-wavelength depolarization-ratio profiling with lidar in Saharan dust over Barbados during SALTRACE 2013 and 2014, Atmos. Chem. Phys., in preparation for this special issue, 2017.

Heintzenberg, J.: The SAMUM-1 experiment over Southern Morocco: overview and introduction, Tellus B, 61, 2–11, doi:10.1111/j.1600-0889.2008.00403.x, 2009.

Hess, M., Koepke, P., and Schult, I.: Optical Properties of Aerosols and Clouds: The Software Package OPAC, Bull. Amer. Meteor. Soc., 79, 831–844, doi:10.1175/1520-0477(1998)079<0831:OPOAAC>2.0.CO;2, 1998.

Hinds, W. C.: Aerosol technology: properties, behavior, and measurement of airborne particles, John Wiley & Sons, 1999.

Hunt, W. H., Winker, D. M., Vaughan, M. A., Powell, K. A., Lucker, P. L., and Weimer, C.: CALIPSO Lidar Description and Performance Assessment, J. Atmos. Oceanic Technol., 26, 1214–1228, doi:10.1175/2009JTECHA1223.1, 2009.

Järvinen, E., Kemppinen, O., Nousiainen, T., Kociok, T., Möhler, O., Leisner, T., and Schnaiter, M.: Laboratory investigations of mineral dust near-backscattering depolarization ratios, J. Quant. Spectrosc. Radiat. Transf., 178, 192–208, doi:10.1016/j.jqsrt.2016.02.003, 2016.

Kaaden, N., Massling, A., Schladitz, A., Müller, T., Kandler, K., Schütz, L., Weinzierl, B., Petzold, A., Tesche, M., Leinert, S., Deutscher, C., Ebert, M., Weinbruch, S., and Wiedensohler, A.: State of mixing, shape factor, number size distribution, and hygroscopic growth of the Saharan anthropogenic and mineral dust aerosol at Tinfou, Morocco, Tellus B, 61, 51–63, doi:10.1111/j.1600-0889.2008.00388.x, 2009.

Kandler, K., Lieke, K., Benker, N., Emmel, C., Küpper, M., Müller-Ebert, D., Scheuvens, D., Schladitz, A., Schütz, L., and Weinbruch, S.: Electron microscopy of particles collected at Praia, Cape Verde, during the Saharan Mineral dust experiment: particle chemistry, shape, mixing state and complex refractive index, Tellus B, 63, 475–496, doi:10.1111/j.1600-0889.2011.00550.x, 2011.

Knippertz, P., Ansmann, A., Althausen, D., Müller, D., Tesche, M., Bierwirth, E., Dinter, T., Müller, T., Von Hoyningen-Huene, W., Schepanski, K., Wendisch, M., Heinold, B., Kandler, K., Petzold, A., Schütz, L., and Tegen, I.: Dust mobilization and transport in the northern Sahara during SAMUM 2006 - a meteorological overview, Tellus B, 61, 12–31, doi:10.1111/j.1600-0889.2008.00380.x, 2009.

Koepke, P., Gasteiger, J., and Hess, M.: Technical Note: Optical properties of desert aerosol with non-spherical mineral particles: data incorporated to OPAC, Atmos. Chem. Phys., 15, 5947–5956, doi:10.5194/acp-15-5947-2015, 2015.

Liu, Z., Omar, A., Vaughan, M., Hair, J., Kittaka, C., Hu, Y., Powell, K., Trepte, C., Winker, D., Hostetler, C., Ferrare, R., and Pierce, R.: CALIPSO lidar observations of the optical properties of Saharan dust: A case study of long-range transport, J. Geophys. Res., 113, D07 207, doi:10.1029/2007JD008878, 2008.

Liu, Z., Vaughan, M., Winker, D., Kittaka, C., Getzewich, B., Kuehn, R., Omar, A., Powell, K., Trepte, C., and Hostetler, C.: The CALIPSO Lidar Cloud and Aerosol Discrimination: Version 2 Algorithm and Initial Assessment of Performance, J. Atmos. Oceanic Technol., 26, 1198–1213, doi:10.1175/2009JTECHA1229.1, 2009.

Liu, Z., Fairlie, T. D., Uno, I., Huang, J., Wu, D., Omar, A., Kar, J., Vaughan, M., Rogers, R., Winker, D., Trepte, C., Hu, Y., Sun, W., Lin, B., and Cheng, A.: Transpacific transport and evolution of the optical properties of Asian dust, J. Quant. Spectrosc. Radiat. Transf., 116, 24–33, doi:10.1016/j.jqsrt.2012.11.011, 2013.

Loth, E.: Drag of non-spherical solid particles of regular and irregular shape, Powder Technol., 182, 342–353, doi:10.1016/j.powtec.2007.06.001, 2008.

Mahowald, N., Albani, S., Kok, J. F., Engelstaeder, S., Scanza, R., Ward, D. S., and Flanner, M. G.: The size distribution of desert dust aerosols and its impact on the Earth system, Aeolian Res., 15, 53–71, doi:10.1016/j.aeolia.2013.09.002, 2014.

Maring, H., Savoie, D. L., Izaguirre, M. A., Custals, L., and Reid, J. S.: Mineral dust aerosol size distribution change during atmospheric transport, J. Geophys. Res. Atmos., 108, 8592, doi:10.1029/2002JD002536, 2003.

Mattis, I., Ansmann, A., Müller, D., Wandinger, U., and Althausen, D.: Dual-wavelength Raman lidar observations of the extinction-to-backscatter ratio of Saharan dust, Geophys. Res. Lett., 29, 20–1–20–4, doi:10.1029/2002GL014721, 2002.

NASA: CALIPSO Lidar Level 2 Aerosol Profile Products Version 3.01, doi:10.5067/CALIOP/CALIPSO/CAL_LID_L2_05kmAPro-Prov-V3-01_L2-003.01, 2010.

Otto, S., Bierwirth, E., Weinzierl, B., Kandler, K., Esselborn, M., Tesche, M., Schladitz, A., Wendisch, M., and Trautmann, T.: Solar radiative effects of a Saharan dust plume observed during SAMUM assuming spheroidal model particles, Tellus B, 61, 270–296, doi:10.1111/j.1600-0889.2008.00389.x, 2009.

Papayannis, A., Amiridis, V., Mona, L., Tsaknakis, G., Balis, D., Bösenberg, J., Chaikovski, A., de Tomasi, F., Grigorov, I., Mattis, I., Mitev, V., Müller, D., Nickovic, S., Pérez, C., Pietruczuk, A., Pisani, G., Ravetta, F., Rizi, V., Sicard, M., Trickl, T., Wiegner, M., Gerding, M., Mamouri, R. E., D'Amico, G., and Pappalardo, G.: Systematic lidar observations of Saharan dust over Europe in the frame of EARLINET (2000–2002), J. Geophys. Res., 113, D10 204, doi:10.1029/2007JD009028, 2008.

Pappalardo, G., Amodeo, A., Apituley, A., Comeron, A., Freudenthaler, V., Linné, H., Ansmann, A., Bösenberg, J., D'Amico, G., Mattis, I., Mona, L., Wandinger, U., Amiridis, V., Alados-Arboledas, L., Nicolae, D., and Wiegner, M.: EARLINET: towards an advanced sustainable European aerosol lidar network, Atmos. Meas. Tech., 7, 2389–2409, doi:10.5194/amt-7-2389-2014, 2014.

Powell, K. A., Hostetler, C. A., Vaughan, M. A., Lee, K.-P., Trepte, C. R., Rogers, R. R., Winker, D. M., Liu, Z., Kuehn, R. E., Hunt, W. H., and Young, S. A.: CALIPSO Lidar Calibration Algorithms. Part I: Nighttime 532-nm Parallel Channel and 532-nm Perpendicular Channel, J. Atmos. Oceanic Technol., 26, 2015–2033, doi:10.1175/2009JTECHA1242.1, 2009.

Prospero, J. M. and Carlson, T. N.: Vertical and areal distribution of Saharan dust over the western equatorial North Atlantic Ocean, J. Geophys. Res, 77, 5255–5265, doi:10.1029/JC077i027p05255, 1972.

Reid, J. S., Kinney, J. E., Westphal, D. L., Holben, B. N., Welton, E. J., Tsay, S., Eleuterio, D. P., Campbell, J. R., Christopher, S. A., Colarco, P. R., Jonsson, H. H., Livingston, J. M., Maring, H. B., Meier, M. L., Pilewskie, P., Prospero, J. M., Reid, E. A., Remer, L. A., Russell, P. B., Savoie, D. L., Smirnov, A., and Tanré, D.: Analysis of measurements of Saharan dust by airborne and ground-based remote sensing methods during the Puerto Rico Dust Experiment (PRIDE), J. Geophys. Res. Atmos., 108, 8586, doi:10.1029/2002JD002493, 2003.

Ryder, C. L., Highwood, E. J., Rosenberg, P. D., Trembath, J., Brooke, J. K., Bart, M., Dean, A., Crosier, J., Dorsey, J., Brindley, H., Banks, J., Marsham, J. H., McQuaid, J. B., Sodemann, H., and Washington, R.: Optical properties of Saharan dust aerosol and contribution from the coarse mode as measured during the Fennec 2011 aircraft campaign, Atmos. Chem. Phys., 13, 303–325, doi:10.5194/acp-13-303-2013, 2013.

Sakai, T., Nagai, T., Zaizen, Y., and Mano, Y.: Backscattering linear depolarization ratio measurements of mineral, sea-salt, and ammonium sulfate particles simulated in a laboratory chamber, Appl. Opt., 49, 4441–4449, doi:10.1364/AO.49.004441, 2010.

Sassen, K.: The Polarization Lidar Technique for Cloud Research: A Review and Current Assessment, Bull. Amer. Meteor. Soc., 72, 1848–1866, doi:10.1175/1520-0477(1991)072<1848:TPLTFC>2.0.CO;2, 1991.

Schütz, L.: Long range transport of desert dust with special emphasis on the Sahara, Ann. N. Y. Acad. Sci., 338, 515–532, doi:10.1111/j.1749-6632.1980.tb17144.x, 1980.

Tsamalis, C., Chédin, A., Pelon, J., and Capelle, V.: The seasonal vertical distribution of the Saharan Air Layer and its modulation by the wind, Atmos. Chem. Phys., 13, 11 235–11 257, doi:10.5194/acp-13-11235-2013, 2013.

Ulanowski, Z., Bailey, J., Lucas, P. W., Hough, J. H., and Hirst, E.: Alignment of atmospheric mineral dust due to electric field, Atmos. Chem. Phys., 7, 6161–6173, doi:10.5194/acp-7-6161-2007, 2007.

Vaughan, M. A., Powell, K. A., Kuehn, R. E., Young, S. A., Winker, D. M., Hostetler, C. A., Hunt, W. H., Liu, Z., McGill, M. J., and Getzewich, B. J.: Fully Automated Detection of Cloud and Aerosol Layers in the CALIPSO Lidar Measurements, J. Atmos. Oceanic Technol., 26, 2034–2050, doi:10.1175/2009JTECHA1228.1, 2009.

Wandinger, U., Tesche, M., Seifert, P., Ansmann, A., Müller, D., and Althausen, D.: Size matters: Influence of multiple scattering on CALIPSO light-extinction profiling in desert dust, Geophys. Res. Lett., 37, L10 801, doi:10.1029/2010GL042815, 2010.

Weinzierl, B., Petzold, A., Esselborn, M., Wirth, M., Rasp, K., Kandler, K., Schütz, L., Koepke, P., and Fiebig, M.: Airborne measurements of dust layer properties, particle size distribution and mixing state of Saharan dust during SAMUM 2006, Tellus B, 61, 96–117, doi:10.1111/j.1600-0889.2008.00392.x, 2009.

Weinzierl, B., Sauer, D., Esselborn, M., Petzold, A., Veira, A., Rose, M., Mund, S., Wirth, M., Ansmann, A., Tesche, M., Groß, S., and Freudenthaler, V.: Microphysical and optical properties of dust and tropical biomass burning aerosol layers in the Cape Verde region - An overview of the airborne in situ and lidar measurements during SAMUM-2, Tellus B, 63, 589–618, doi:10.1111/j.1600-0889.2011.00566.x, 2011.

Weinzierl, B., Ansmann, A., Prospero, J. M., Althausen, D., Benker, N., Chouza, F., Dollner, M., Farrell, D., Fomba, W. K., Freudenthaler, V., Gasteiger, J., Groß, S., Haarig, M., Heinold, B., Kandler, K., Kristensen, T. B., Mayol-Bracero, O. L., Müller, T., Reitebuch, O., Sauer, D., Schäfler, A., Schepanski, K., Spanu, A., Tegen, I., Toledano, C., and Walser, A.: The Saharan Aerosol Long-range Transport and Aerosol-Cloud-Interaction Experiment (SALTRACE): overview and selected highlights, Bull. Amer. Meteor. Soc., in review, 2016.

Wiegner, M., Groß, S., Freudenthaler, V., Schnell, F., and Gasteiger, J.: The May/June 2008 Saharan dust event over Munich: Intensive aerosol parameters from lidar measurements, J. Geophys. Res., 116, D23 213, doi:10.1029/2011JD016619, 2011.

Winker, D. M., Vaughan, M. A., Omar, A., Hu, Y., Powell, K. A., Liu, Z., Hunt, W. H., and Young, S. A.: Overview of the CALIPSO Mission and CALIOP Data Processing Algorithms, J. Atmos. Oceanic Technol., 26, 2310–2323, doi:10.1175/2009JTECHA1281.1, 2009.

Yang, W., Marshak, A., Kostinski, A. B., and Várnai, T.: Shape-induced gravitational sorting of Saharan dust during transatlantic voyage: Evidence from CALIOP lidar depolarization measurements, Geophys. Res. Lett., 40, 3281–3286, doi:10.1002/grl.50603, 2013.

Young, S. A.: Uncertainty Analysis for Particulate Backscatter, Extinction and Optical Depth Retrievals reported in the CALIPSO Level 2, Version 3 Data Release, https://eosweb.larc.nasa.gov/sites/default/files/project/calipso/CALIOP_Version3_Extinction_Error_Analysis.pdf, 2010.

Yurkin, M. A. and Hoekstra, A. G.: The discrete-dipole-approximation code ADDA: Capabilities and known limitations, J. Quant. Spectrosc. Radiat. Transf., 112, 2234–2247, doi:10.1016/j.jqsrt.2011.01.031, 2011.